

# **First Search for Heavy Neutral Leptons with IceCube DeepCore**

## **Dissertation**

zur Erlangung des akademischen Grades  
doctor rerum naturalium  
(Dr. rer. nat.)

im Fach: Physik  
Spezialisierung: Experimentalphysik

eingereicht an der  
Mathematisch-Naturwissenschaftlichen Fakultät  
der Humboldt-Universität zu Berlin

von

**Leander Fischer M. Sc.**  
geboren am 24. Oktober 1992  
in Heidelberg

Präsidentin der Humboldt-Universität zu Berlin  
Prof. Dr. Julia von Blumenthal

Dekanin der Mathematisch-Naturwissenschaftlichen Fakultät  
Prof. Dr. Caren Tischendorf

**Copyright Notice**

This book is released into the public domain using the CC-BY-4.0 code.

To view a copy of the CC-BY-4.0 code, visit:

<https://creativecommons.org/licenses/by/4.0/>

**Colophon**

This document was typeset with the help of KOMA-Script and L<sup>A</sup>T<sub>E</sub>X using the open-source kaobook template class.

The source code of this thesis is available at:

[https://github.com/LeanderFischer/phd\\_thesis](https://github.com/LeanderFischer/phd_thesis)

# Todo list

highlight a few more neutrino related open questions, to circle back to related to the HNL searches maybe? (YELLOW) . . . . .	4
add Majorana condition and mention what this means for interactions (LNV of 2) (ORANGE) . . . . .	5
Discuss lepton number conservation (pure dirac) and lepton number violation (dirac+majorana) (ORANGE) . . . . .	5
elaborate on Leptogenesis in $\nu$ MSM and sterile neutrino DM, or link some papers? (ORANGE) . . . . .	6
I think here I'd want the extended leptonic EW lagrangien, so I can explain the mass mixing and the interactions it opens up (RED) . . . . .	6
mention KENU, Belle, L3 in the text and add references (RED) . . . . .	7
mention PSI, LSND, NA3 in the text and add references (RED) . . . . .	8
mention the Z boson decay results from DELPHI (because they are strong in Utau4, too (RED)) . . . . .	8
Say something about atmospheric neutrino flux uncertainties, based on recent JP/Anatoli papers. (YELLOW) . . . . .	12
say something about matter effect? (ORANGE) . . . . .	13
say something about mass ordering? (ORANGE) . . . . .	13
SB: there are more properties than just these. Somehow need a half sentence that explains why these are particularly important to single out (see ice papers for inspiration) (RED) . . . . .	20
CL: maybe define what absorption and scattering lengths are? they are defined differently so this invites a comparison that is not so obvious (RED) . . . . .	20
Add reference for the dust layer! Maybe also from the ice paper? mention/cite dust logger paper/procedure? (RED) . . . . .	20
Add angular profile plot (Summer agrees!) (create one based on Leif Radel as Alex did) (RED) . . . . .	25



# Contents

<b>Contents</b>	<b>v</b>
<b>1 Standard Model Neutrinos and Beyond</b>	<b>1</b>
1.1 The Standard Model . . . . .	1
1.1.1 Fundamental Fields . . . . .	1
1.1.2 Electroweak Symmetry Breaking . . . . .	2
1.1.3 Fermion Masses . . . . .	3
1.1.4 Leptonic Weak Interactions after Symmetry Breaking . . . . .	3
1.2 Beyond the Standard Model . . . . .	3
1.2.1 Mass Mechanisms . . . . .	4
1.2.2 Minimal Extensions and the $\nu$ MSM . . . . .	5
1.2.3 Observational Avenues for Right-Handed Neutrinos . . . . .	6
1.3 Atmospheric Neutrinos as Source of Heavy Neutral Leptons . . . . .	11
1.3.1 Production of Neutrinos in the Atmosphere . . . . .	11
1.3.2 Neutrino Oscillations . . . . .	12
1.3.3 Neutrino Interactions with Nuclei . . . . .	14
1.3.4 Heavy Neutral Lepton Production and Decay . . . . .	15
<b>2 The IceCube Neutrino Observatory</b>	<b>19</b>
2.1 Detector Components . . . . .	19
2.1.1 Digital Optical Modules and the Antarctic Ice . . . . .	20
2.1.2 IceCube Main-Array . . . . .	21
2.1.3 DeepCore Sub-Array . . . . .	22
2.2 Particle Propagation in Ice . . . . .	22
2.2.1 Cherenkov Effect . . . . .	22
2.2.2 Energy Losses . . . . .	23
2.3 Event Morphologies . . . . .	25
<b>Bibliography</b>	<b>27</b>



# Standard Model Neutrinos and Beyond

# 1

## 1.1 The Standard Model

The SM of particle physics is a Yang-Mills theory [1] providing very accurate predictions of weak, strong, and *electromagnetic* (EM) interactions. It is a relativistic quantum field theory that relies on gauge invariance, where all matter is made up of fermions, which are divided into quarks and leptons, and bosons describe the interactions between the fermions that have to fulfil the overall symmetry of the theory. Leptons are excitations of Dirac-type fermion fields.

The initial idea of the theory is associated with the works of Weinberg [2], Glashow [3], and Salam [4], that proposed a unified description of EM and weak interactions as a theory of a spontaneously broken  $SU(2) \times U(1)$  symmetry for leptons, predicting a neutral massive vector boson  $Z^0$ , a massive charged vector boson  $W^\pm$ , and a massless photon  $\gamma$  as the gauge bosons. The Higgs mechanism [5], describing the breaking of the symmetry, predicts the existence of an additional scalar particle, the Higgs boson, giving the  $W^\pm$  and  $Z^0$  bosons their mass. The Higgs boson was discovered in 2012 at the LHC [6, 7].

Gell-Mann and Zweig proposed the quark model in 1964 [8, 9], which was completed by the discovery of non-abelian gauge theories [10] to form the  $SU(3)$  symmetry of the strong interaction called *quantum chromodynamics* (QCD). QCD describes the interaction between quarks and gluons which completed the full picture of the SM in the mid-1970s. Together with the electroweak theory, the SM is a  $SU(3)_C \times SU(2)_L \times U(1)_Y$  local gauge symmetry, with the conserved quantities  $C$ , *color*,  $L$ , *left-handed chirality*, and  $Y$ , *weak hypercharge*.

In the following, the basic properties of the SM are described, following the derivations of [11, 12].

### 1.1.1 Fundamental Fields

Fermions in the SM are Weyl fields with either *left-handed* (LH) or *right-handed* (RH) chirality, meaning they are eigenvectors of the chirality operator  $\gamma_5$  with  $\gamma_5 \psi_{R/L} = \pm \psi_{R/L}$ . Only LH particles transform under  $SU(2)_L$ . The Higgs field is a complex scalar field, a doublet of  $SU(2)_L$ , which is responsible for the spontaneous symmetry breaking of  $SU(2)_L \times U(1)_Y$  to  $U(1)_{EM}$ . Local gauge transformations of the fields are given by

$$\psi \rightarrow e^{ig\theta^a(x)T^a} \psi, \quad (1.1)$$

where  $g$  is the coupling constant,  $\theta^a(x)$  are the parameters of the transformation, and  $T^a$  are the generators of the group, with  $a$  counting them. The number of bosons is dependent on the generators of the symmetry groups, while the strength is defined by the coupling constants. There are eight massless gluons corresponding to the generators of the  $SU(3)_C$  group. These

1.1	The Standard Model	1
1.2	Beyond the Standard Model . . . . .	3
1.3	Atmospheric Neutrinos as Source of Heavy Neutral Leptons . . .	11

[1]: Yang et al. (1954), "Conservation of Isotopic Spin and Isotopic Gauge Invariance"

[2]: Weinberg (1967), "A Model of Leptons"

[3]: Glashow (1961), "Partial-symmetries of weak interactions"

[5]: Higgs (1964), "Broken symmetries, massless particles and gauge fields"

[6]: Chatrchyan et al. (2012), "Observation of a New Boson at a Mass of 125 GeV with the CMS Experiment at the LHC"

[7]: Aad et al. (2012), "Observation of a new particle in the search for the Standard Model Higgs boson with the ATLAS detector at the LHC"

[8]: Gell-Mann (1964), "A Schematic Model of Baryons and Mesons"

[9]: Zweig (1964), "An  $SU(3)$  model for strong interaction symmetry and its breaking. Version 2"

[11]: Giunti et al. (2007), *Fundamentals of Neutrino Physics and Astrophysics*

[12]: Schwartz (2013), *Quantum Field Theory and the Standard Model*

mediate the strong force which conserves color charge. The  $W_1, W_2, W_3$ , and  $B$  boson fields of the  $SU(2)_L \times U(1)_Y$  group are mixed into the massive bosons through spontaneous symmetry breaking as

$$W^\pm = \frac{1}{\sqrt{2}}(W_1 \mp iW_2) \quad (1.2)$$

and

$$Z^0 = \cos \theta_W W_3 - \sin \theta_W B, \quad (1.3)$$

with  $\theta_W$  being the *Weinberg angle*. The massless photon field is given by

$$A = \sin \theta_W W_3 + \cos \theta_W B \quad (1.4)$$

and its conserved quantity is the EM charge  $Q$ , which depends on the weak hypercharge,  $Y$ , and the third component of the weak isospin,  $T_3$ , as  $Q = T_3 + Y/2$ .

	Type			Q
quarks	u	c	t	+2/3
	d	s	b	-1/3
leptons	$\nu_e$	$\nu_\mu$	$\nu_\tau$	0
	e	$\mu$	$\tau$	-1

**Table 1.1:** Fermions in the Standard Model. Shown are all three generations of quarks and leptons with their electric charge  $Q$ .

Fermions are divided into six quarks and six leptons. Weak, strong, and EM force act on the quarks, and they are always found in bound form as baryons or mesons. Leptons do not participate in the strong interaction and only the electrically charged leptons are massive and are effected by the EM force, while neutrinos are massless and only interact via the weak force. Each charged lepton has an associated neutrino, which it interacts with in *charged-current* (CC) weak interactions, that will be explained in more detail in Section 1.1.4. The fermions are listed in Table 1.1.

### 1.1.2 Electroweak Symmetry Breaking

To elaborate the process of spontaneous symmetry breaking through which the gauge bosons of the weak interaction acquire their masses, the Lagrangian of the Higgs field is considered as

$$\mathcal{L}_{\text{Higgs}} = (D_\mu \Phi^\dagger)(D^\mu \Phi) - \lambda \left( \Phi^\dagger \Phi - \frac{v^2}{2} \right)^2, \quad (1.5)$$

with parameters  $\lambda$  and  $v$ , where  $\lambda$  is assumed to be positive.  $\Phi$  is the Higgs doublet, which is defined as

$$\Phi = \begin{pmatrix} \Phi^+ \\ \Phi^0 \end{pmatrix}, \quad (1.6)$$

with the charged component  $\Phi^+$  and the neutral component  $\Phi^0$ . The covariant derivative is given by

$$D_\mu = \partial_\mu - ig_2 \frac{\sigma^i}{2} W_\mu^i - \frac{1}{2} ig_1 B_\mu, \quad (1.7)$$

with the Pauli matrices  $\sigma^i$  and the gauge boson fields  $W_\mu^i$  and  $B_\mu$  of the  $SU(2)_L$  and  $U(1)_Y$  groups, respectively. The coupling constants  $g_2$  and  $g_1$  are the respective coupling constants which are related to the Weinberg angle as  $\tan \theta_W = \frac{g_1}{g_2}$ . The Higgs potential has a non-zero *vacuum expectation value* ( $v$ ) at the minimum of the potential at  $\Phi^\dagger \Phi = \frac{v^2}{2}$ . Since the vacuum is electrically neutral, it can only come from a neutral component of the Higgs



doublet as

$$\Phi_{\text{vev}} = \frac{1}{\sqrt{2}} \begin{pmatrix} 0 \\ v \end{pmatrix}. \quad (1.8)$$

### 1.1.3 Fermion Masses

The mass term for charged fermions with spin-1/2 is given by

$$\mathcal{L}_{\text{Dirac}} = m(\bar{\Psi}_R \Psi_L - \bar{\Psi}_L \Psi_R), \quad (1.9)$$

composed of the product of LH and RH Weyl spinors  $\Psi_{L/R}$ . This term is not invariant under  $SU(2)_L \times U(1)_Y$  gauge transformations, but adding a Yukawa term

$$\mathcal{L}_{\text{Yukawa}} = -Y^e \bar{L}_L \Phi e_R + h.c., \quad (1.10)$$

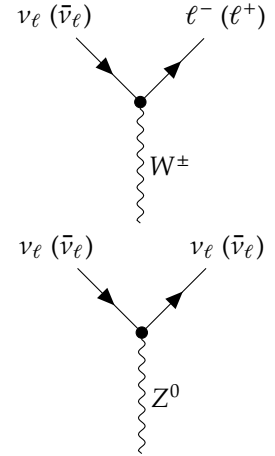
coupling the fermion fields  $e_R$  to the Higgs field  $\Phi$ , recovers the invariance and gives the fermions their masses. Here,  $Y^e$  is the Yukawa coupling constant and  $\bar{L}_L$  is the  $SU(2)_L$  doublet. With the vev, this results in the mass term for the charged leptons and down-type quarks of  $-m_e(\bar{e}_L e_R + \bar{e}_R e_L)$  with  $m_e = \frac{Y^e v}{\sqrt{2}}$ . With  $\tilde{\Phi} = i\sigma_2 \Phi^*$ , a similar Yukawa term can be written as  $-Y^u \bar{L}_L \tilde{\Phi} u_R + h.c.$ , which leads to the masses of the up-type quarks.

### 1.1.4 Leptonic Weak Interactions after Symmetry Breaking

After the spontaneous symmetry breaking, the leptonic part of the electroweak Lagrangian can be written as

$$\begin{aligned} \mathcal{L}_{\text{EW}}^\ell = & \frac{g}{\sqrt{2}} W^+ \sum_{\alpha=e,\mu,\tau} \bar{\nu}_\alpha \gamma^\mu P_L \ell_\alpha + \frac{g}{4c_w} Z \\ & \times \left\{ \sum_{\alpha=e,\mu,\tau} \bar{\nu}_\alpha \gamma^\mu P_L \nu_\alpha + \sum_\alpha \bar{\ell}_\alpha \gamma^\mu [2s_w^2 P_R - (1 - 2s_w^2) P_L] \ell_\alpha \right\} + h.c., \end{aligned} \quad (1.11)$$

where  $c_w \equiv \cos \theta_w$ ,  $s_w \equiv \sin \theta_w$ ,  $P_L$  and  $P_R$  are the left and right projectors, respectively, while  $\nu_\alpha$  and  $\ell_\alpha$  are the neutrino and charged lepton weak eigenstates. The  $W^\pm$  and  $Z$  bosons are the massive gauge bosons of the weak interaction. The large boson masses  $m_W \sim 80 \text{ GeV}$  and  $m_Z \sim 90 \text{ GeV}$  result in a short range of the force of about  $1 \times 10^{-18} \text{ m}$ . Interactions carried out by the  $W^\pm$  bosons are called *charged current (CC)* interactions, as they propagate a charge, therefore changing the interacting lepton to its charged/neutral counterpart. *Neutral current (NC)* interactions are those mediated by the  $Z^0$  boson, where no charge is transferred. NC interactions couple neutrinos to neutrinos and charged leptons to charged leptons, but not to each other. The Feynman diagrams for CC and NC interactions are shown in Figure 1.1.



**Figure 1.1:** Feynman diagrams of charged-current (top) and neutral-current (bottom) neutrino weak interactions, modified from [13].

## 1.2 Beyond the Standard Model

The fundamentals of the SM described above **are not** enough to explain all observed phenomena. Gravity cannot be explained by the SM, as it is incompatible with general relativity, neither can some of the cosmological observations like DM, and the matter-antimatter asymmetry be explained. But most importantly, the SM does not predict neutrinos to have mass, which

is experimentally proven by neutrino oscillations, so some extension to the SM is needed in order to explain the observed phenomena.

[14]: Deruelle et al. (2018), *Relativity in Modern Physics*

The standard cosmological model  $\Lambda$ CDM [14] assumes that equal amounts of matter and anti-matter were produced in the early universe. However, the universe today is dominantly made up of matter. This BAU can be measured by the difference between the number densities of baryons and anti-baryons normalized to the number density of photons as

$$\eta_B = \frac{n_B - n_{\bar{B}}}{n_\gamma}, \quad (1.12)$$

where  $n_B$ ,  $n_{\bar{B}}$ , and  $n_\gamma$  are the number densities of baryons, anti-baryons, and photons, respectively. Baryons are the dominant component with  $\eta_B$  being observed to be at the order of  $10^{-9}$  [15]. Leptogenesis and EW baryogenesis are scenarios that could explain this phenomenon, where the former could be realized by the existence of heavy RH neutrinos [16].

[15]: Workman et al. (2022), "Review of Particle Physics"

[16]: Fukugita et al. (1986), "Baryogenesis without grand unification"

[17]: Davis et al. (1968), "Search for Neutrinos from the Sun"

[18]: Fukuda et al. (1998), "Evidence for Oscillation of Atmospheric Neutrinos"

[19]: Ahmad et al. (2002), "Direct Evidence for Neutrino Flavor Transformation from Neutral-Current Interactions in the Sudbury Neutrino Observatory"

[20]: Alam et al. (2021), "Completed SDSS-IV extended Baryon Oscillation Spectroscopic Survey: Cosmological implications from two decades of spectroscopic surveys at the Apache Point Observatory"

[21]: Aghanim et al. (2020), "Planck2018 results: VI. Cosmological parameters"

[22]: Aker et al. (2022), "Direct neutrino-mass measurement with sub-electronvolt sensitivity"

highlight a few more neutrino related open questions, to circle back to related to the HNL searches maybe? (YELLOW)

The observation of neutrino flavor conversions and neutrino oscillations in a multitude of experiments [17–19] is the strongest evidence for physics *beyond the standard model (BSM)* measured in laboratories to date. The observation that neutrinos change their flavor while they propagate through space can only be explained, if at least two neutrinos have a non-zero mass. From those measurements we know the mass differences are very small as compared to the lepton masses, but neither their existence, nor their smallness is predicted by the SM. There are upper limits on the sum of all neutrino masses from cosmological observations at 1.2 eV [20, 21] and at 0.8 eV from the KATRIN experiment [22]. Adding RH neutrino states to the theory could explain the origin of the observed non-zero neutrino masses and could be tested for by searching for corresponding signatures in experiments.

### 1.2.1 Mass Mechanisms

Since there are no RH neutrinos in the SM, the mass mechanism described in Section 1.1.3, which couples the Higgs field to LH and RH Weyl fields, predicts the LH neutrinos to be massless. From experimental observations it is known that at least two of the three neutrino generations need to have a non-zero mass. Assuming the existence of RH neutrinos fields  $\nu_R$ , one way of producing the neutrino masses is by adding a Yukawa coupling term similar to the one for up-type quarks mentioned in Section 1.1.3, to write the full Yukawa Lagrangian as

$$\mathcal{L}_{\text{Yukawa}} = -Y_{ij}^e \bar{L}_L^i \Phi e_R^j - Y_{ij}^\nu \bar{L}_L^i \tilde{\Phi} \nu_R^j + h.c., \quad (1.13)$$

with  $i, j$  running over the three generations of leptons  $e, \mu$ , and  $\tau$ , and  $Y^e$  and  $Y^\nu$  being the Yukawa coupling matrices. Diagonalizing the Yukawa coupling matrices through unitary transformations  $U^e$  and  $U^\nu$  leads to the **Dirac mass term** in the mass basis as

$$\mathcal{L}_{\text{Dirac}}^{\text{mass}} = \frac{v}{\sqrt{2}} (\bar{e}_L M_e e_R - \bar{\nu}_L M_\nu \nu_R), \quad (1.14)$$

where  $M_e$  and  $M_\nu$  are the diagonal mass matrices of leptons and neutrinos, respectively. A purely Dirac mass term would not explain the smallness of

the neutrino masses in a straightforward way. Only fine-tuning the Yukawa coupling constants to small values would lead to small neutrino masses.

An additional way of generating neutrino masses is by adding a Majorana mass term of the form

$$\mathcal{L}_{\text{Majorana}} = -\frac{1}{2}M_{ij}(\nu_R^i)^c \nu_R^j + h.c. , \quad (1.15)$$

with  $M_{ij}$  being the Majorana mass matrix and the indices  $i, j$  running over all  $n_R$  RH neutrino generations. The superscript  $c$  denotes the charge conjugate field. Combining the charge conjugated RH neutrino fields with the LH neutrino fields as

$$N = \begin{pmatrix} \nu_L \\ \nu_R^c \end{pmatrix} , \quad (1.16)$$

with  $\nu_R$  containing the  $n_R$  RH fields. The full neutrino mass Lagrangian is then given by the combined **Dirac and Majorana mass term** as

$$\mathcal{L}_{\text{Dirac+Majorana}}^{\text{mass},\nu} = \frac{1}{2}N^T \hat{C} M^{\text{D+M}} N + h.c. , \quad (1.17)$$

and the mass matrix is given by

$$M^{\text{D+M}} = \begin{pmatrix} 0 & (M^D)^T \\ M^D & M^R \end{pmatrix} . \quad (1.18)$$

On top of explaining the origin of neutrino masses itself, a combined Dirac and Majorana mass term could also solve the question of their smallness. If the mass of the RH neutrinos is very large, the masses of the active neutrino flavors is suppressed, which is known as *see-saw mechanism*.

### 1.2.2 Minimal Extensions and the $\nu$ MSM

So far we have described neutrinos in their flavor eigenstates, which are relevant for weak interactions, where the three weak flavor states  $\nu_e, \nu_\mu$ , and  $\nu_\tau$  are related to the charged leptons they interact with in CC interactions. In order to *just* explain the three oscillating flavor eigenstates, three mass states are needed, which are related to the flavor eigenstates by the unitary,  $3 \times 3$  Pontecorvo-Maki-Nakagawa-Sakata (PMNS) mixing matrix  $U$ , where the flavor states are a superposition of the mass states as

$$|\nu_\alpha\rangle = \sum_k U_{\alpha k}^* |\nu_k\rangle , \quad (1.19)$$

with the weak flavor states  $|\nu_\alpha\rangle$ ,  $\alpha = e, \mu, \tau$ , and the mass states  $|\nu_k\rangle$  with  $k = 1, 2, 3$ . In its generic form the PMNS matrix is given by

$$U = \begin{pmatrix} U_{e1} & U_{e2} & U_{e3} \\ U_{\mu1} & U_{\mu2} & U_{\mu3} \\ U_{\tau1} & U_{\tau2} & U_{\tau3} \end{pmatrix} , \quad (1.20)$$

which will be the basis for the discussion of neutrino oscillations in Section 1.3.2.

This however is not enough to explain the neutrino masses observed in oscillation experiments. The most minimal model required to give rise to two non-zero active neutrino masses, is an additional two RH neutrinos,

add Majorana condition and mention what this means for interactions (LNV of 2) (ORANGE)

Discuss lepton number conservation (pure dirac) and lepton number violation (dirac+majorana) (ORANGE)

[23]: Asaka et al. (2005), “The nuMSM, dark matter and neutrino masses”

[24]: Asaka et al. (2005), “The  $\nu$ MSM, dark matter and baryon asymmetry of the universe”

elaborate on Leptogenesis in  $\nu$ MSM and sterile neutrino DM, or link some papers? (ORANGE)

[25]: Minkowski (1977), “ $\mu \rightarrow e \gamma$  at a rate of one out of  $10^9$  muon decays?”

[26]: Yanagida (1980), “Horizontal Symmetry and Masses of Neutrinos”

[27]: Glashow (1980), “The Future of Elementary Particle Physics”

[28]: Gell-Mann et al. (1979), “Complex Spinors and Unified Theories”

[29]: Mohapatra et al. (1980), “Neutrino Mass and Spontaneous Parity Nonconservation”

I think here I'd want the extended leptonic EW lagrangien, so I can explain the mass mixing and the interactions it opens up (RED)

[30]: Aartsen et al. (2020), “eV-Scale Sterile Neutrino Search Using Eight Years of Atmospheric Muon Neutrino Data from the IceCube Neutrino Observatory”

[13]: Trettin (2023), “Search for eV-scale sterile neutrinos with IceCube DeepCore”

[31]: Tastet et al. (2021), “Reinterpreting the ATLAS bounds on heavy neutral leptons in a realistic neutrino oscillation model”

assuming the mass of the lightest SM neutrino is zero. If the additional neutrino states have masses  $\gg \text{eV}$  they are referred to as HNL, which are almost sterile, with a small mass mixing with the active neutrinos.

But the SM also fails to explain additional observations of physics beyond the standard model (BAU, DM), which could be solved by the *neutrino minimal standard model* ( $\nu$ MSM) [23, 24]. In the  $\nu$ MSM, three RH neutrinos are added, where two of them are heavy, to explain the observed neutrino masses and oscillations, and a third one is light and serves as a DM candidate. The mixing between mass and flavor eigenstates is then described by an extended 6x6 mixing matrix as

$$\begin{pmatrix} \nu_e \\ \nu_\mu \\ \nu_\tau \\ N_1 \\ N_2 \\ N_3 \end{pmatrix} = \begin{pmatrix} U_{e1} & U_{e2} & U_{e3} & U_{e4} & U_{e5} & U_{e6} \\ U_{\mu1} & U_{\mu2} & U_{\mu3} & U_{\mu4} & U_{\mu5} & U_{\mu6} \\ U_{\tau1} & U_{\tau2} & U_{\tau3} & U_{\tau4} & U_{\tau5} & U_{\tau6} \\ U_{N_11} & U_{N_12} & U_{N_13} & U_{N_14} & U_{N_15} & U_{N_16} \\ U_{N_21} & U_{N_22} & U_{N_23} & U_{N_24} & U_{N_25} & U_{N_26} \\ U_{N_31} & U_{N_32} & U_{N_33} & U_{N_34} & U_{N_35} & U_{N_36} \end{pmatrix} \begin{pmatrix} \nu_1 \\ \nu_2 \\ \nu_3 \\ \nu_4 \\ \nu_5 \\ \nu_6 \end{pmatrix}, \quad (1.21)$$

where  $N_i$  and  $\nu_{i+3}$  ( $i \in [1, 2, 3]$ ) are the sterile flavor states and the additional RH mass states, respectively. In the  $\nu$ MSM, the two heavy RH neutrinos generate the active neutrino masses through the type I seesaw mechanism [25–29], where they are assumed to be SM scalars and couple to the Higgs field as such.

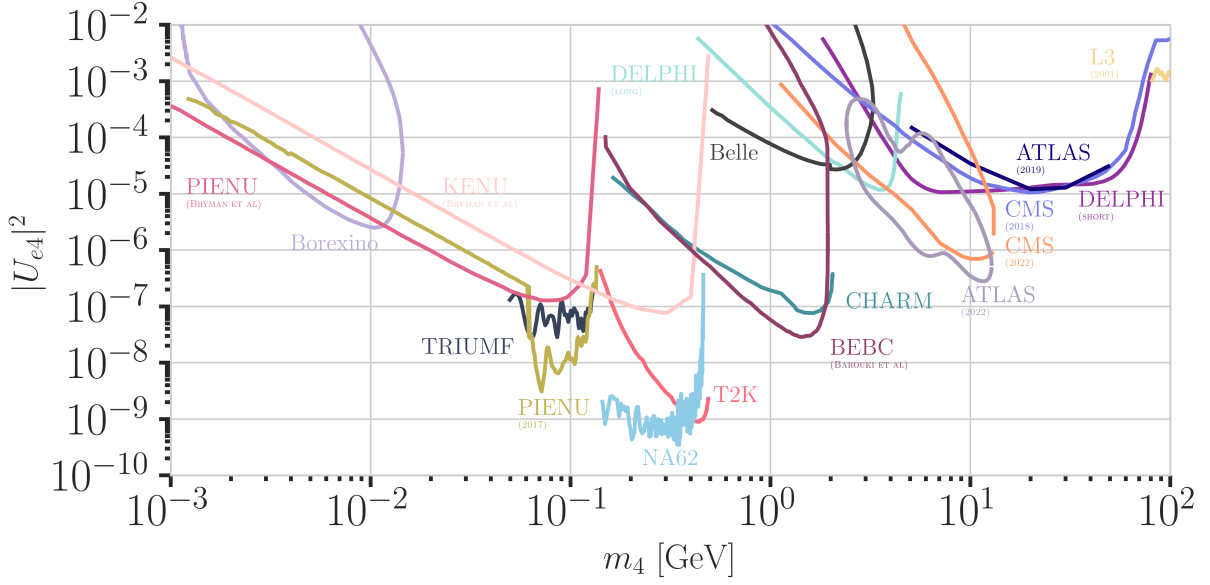
### 1.2.3 Observational Avenues for Right-Handed Neutrinos

If the RH neutrinos have masses at the eV scale, they can be observed through distortion effects in measurements of neutrino oscillation experiments. Several analyses looking for these so-called light sterile neutrinos exist in IceCube, where [30] is using atmospheric neutrinos in the higher energy range of 500 GeV to 10 000 GeV and [13] is using the lower energy region of 6 GeV to 156 GeV. The latter work includes a detailed description of the expected oscillation effects and the various anomalies observed in oscillation experiments that could be explained by the existence of a light sterile neutrino, which is not covered in this work.

Here, the focus will be on heavy RH neutrinos, interchangeably also called heavy sterile neutrinos, or HNLs. A defining property is that they are too massive to be produce in oscillations and to be observed as distortions thereof. Several ways to observe HNLs are possible through direct production and decay experiments, which will be discussed in the following. Most of the existing searches assume the minimal model, where only one coupling between the new mass states and the SM neutrinos is non-zero and the coupling is just through mass mixing in a type I seesaw scenario, but more complex scenarios are of course also possible and might produce various additional signatures, or stronger signals.

In general, the constraints discussed in the following are based on models, where only the coupling between the HNL and one SM flavor is non-zero. While this is the straight forward approach to test the mixing parameters individually, this might make the constraints stronger than they would be in a more complex scenario, where the HNLs couple to more than one SM flavor as was show in [31] for collider bounds.

## Extracted Beamline Searches



**Figure 1.2:** Current leading  $|U_{e4}|^2 - m_4$  limits from PIENU [32, 33], BOREXINO [34], KENU, TRIUMF [35], NA62 [36], T2K [37], DELPHI [38], BEBC [39], Belle, L3, CHARM [40], ATLAS [41, 42], CMS [43, 44], and NuTeV [45]. Modified from [3] in the text and add references (RED)

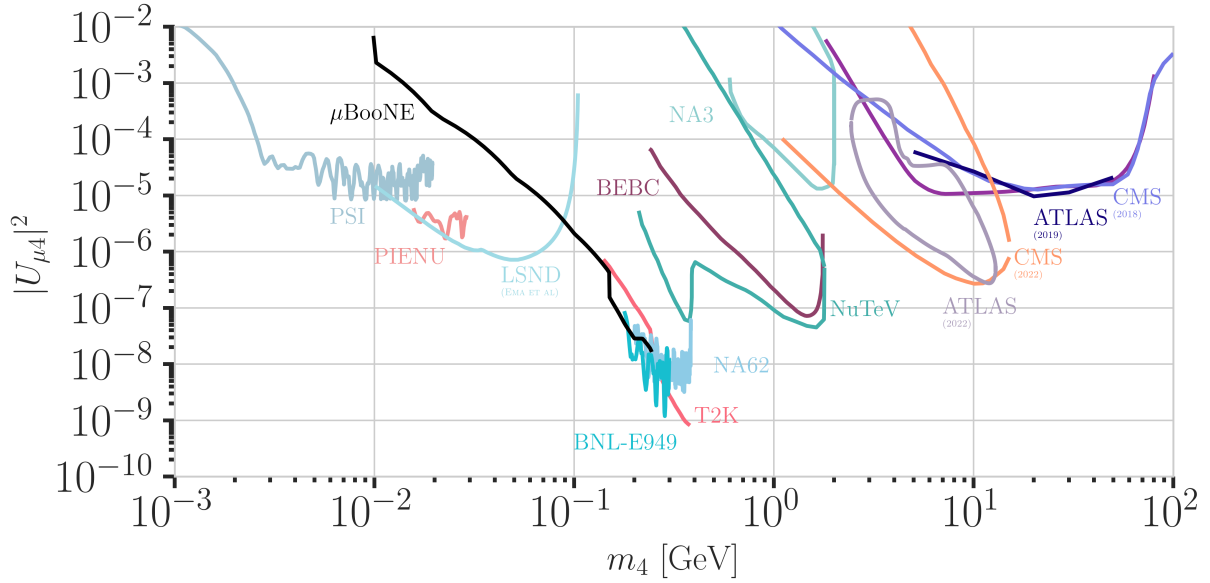
Protons interacting with a target or a beam dump can produce pions, kaons, and heavy-quark hadrons, whose subsequent decays would also produce HNLs. The energies of the HNLs produced in those interactions are between 1 MeV and 4 GeV and could decay at several distances, depending on their lifetime, which is model dependent. Experiments along the extracted beamline, which are using a spectrometer with particle identification, can search for unique decay signatures at displaced vertices. Example signatures are  $\nu_4 \rightarrow l_\alpha \pi$ ,  $\nu_4 \rightarrow l_\alpha^+ l_\alpha^-$ , or  $\nu_4 \rightarrow \nu \pi^0$  (or other neutral mesons), which cannot be explained by SM neutrinos. Depending on the decay channel, a specific mixing can be probed. The other way of searching for HNLs with these interactions is to look for peaks in the missing mass spectrum, measured around the production vertex at the target, which usually is not possible for beam dumps, as the beam dump region is not calorimetrically instrumented.

HNL search pioneer work was done by experiments at extracted beam lines, with first results from *PS191* [47] and *CHARM* [40], reporting bounds from direct production and decay of HNLs for  $|U_{e4}|^2$ ,  $|U_{\mu 4}|^2$ , and combinations of them, at masses from 10 MeV to 500 MeV at orders of  $10^{-3}$  to  $10^{-6}$ . Since then, there has been and still is a large activity of searches for HNLs at extracted beamlines and the strongest bounds on  $|U_{e4}|^2$  and  $|U_{\mu 4}|^2$  are currently set by *PIENU* [32, 33, 48], *TRIUMF* [35], *NA62* [36], *T2K* [37], *BNL-E949* [49], *MicroBooNE* [50], and *NuTeV* [45] in the mass range from 1 MeV to 4 GeV, reaching from  $10^{-4}$  at the lower mass to  $10^{-9}$  at 4 at the highest masses. The current strongest bounds are shown in Figure 1.2 and Figure 1.3, which also shows bounds from other experiments, which will be discussed in the following.

Especially noteworthy are the results of analyses probing the mixing with the third lepton generation,  $|U_{\tau 4}|^2$ , from *NOMAD* [51] and reinterpretations of the *CHARM* results and the *BEBC* results in the context of the mixing

- [47]: Bernardi et al. (1986), “Search for Neutrino Decay”
- [40]: Bergsma et al. (1983), “A Search for Decays of Heavy Neutrinos”
- [32]: Bryman et al. (2019), “Constraints on Sterile Neutrinos in the MeV to GeV Mass Range”
- [33]: Aguilar-Arevalo et al. (2018), “Improved search for heavy neutrinos in the decay  $\pi \rightarrow e \nu$ ”
- [48]: Ito et al. (2021), “Search for heavy neutrinos in  $\pi^+ \rightarrow \mu^+ \nu$  decay and status of lepton universality test in the PIENU experiment”
- [35]: Britton et al. (1992), “Improved search for massive neutrinos in  $\pi^+ \rightarrow e^+ \nu$  decay”
- [36]: Parkinson et al. (2022), “Search for heavy neutral lepton production at the NA62 experiment”
- [37]: Abe et al. (2019), “Search for heavy neutrinos with the T2K near detector ND280”
- [49]: Artamonov et al. (2015), “Search for heavy neutrinos in  $K^+ \rightarrow \mu^+ \nu_H$  decays”
- [50]: Abratenko et al. (2024), “Search for Heavy Neutral Leptons in Electron-Positron and Neutral-Pion Final States with the MicroBooNE Detector”
- [45]: Vaitaitis et al. (1999), “Search for neutral heavy leptons in a high-energy neutrino beam”
- [51]: Astier et al. (2001), “Search for heavy neutrinos mixing with tau neutrinos”





**Figure 1.3:** Current leading  $|U_{\mu 4}|^2 - m_4$  limits from PSI ,  $\mu$ BooNE [50], PIENU [32], LSND , BNL-E949 [49], NA62 [36], T2K [37], BEBC [54], ATLAS [41, 42], CMS [43, 44], NuTeV [45], and NA3 . Modified from [46]. Modified from [46].

[39]: Barouki et al. (2022), “Blast from the past II: Constraints on heavy neutral leptons from the BEBC WA66 beam dump experiment”

[52]: Orloff et al. (2002), “Limits on the mixing of tau neutrino to heavy neutrinos”

[53]: Boiarska et al. (2021), “Constraints from the CHARM experiment on heavy neutral leptons with tau mixing”

mention PSI, LSND, NA3 in the text and add references (RED)

[41]: Aad et al. (2019), “Search for heavy neutral leptons in decays of W bosons produced in 13 TeV  $pp$  collisions using prompt and displaced signatures with the ATLAS detector”

[42]: Aad et al. (2023), “Search for Heavy Neutral Leptons in Decays of W Bosons Using a Dilepton Displaced Vertex in  $\sqrt{s} = 13\text{TeV}$   $pp$  Collisions with the ATLAS Detector”

[43]: Sirunyan et al. (2018), “Search for heavy neutral leptons in events with three charged leptons in proton-proton collisions at  $\sqrt{s} = 13\text{ TeV}$ ”

[44]: Tumasyan et al. (2022), “Search for long-lived heavy neutral leptons with displaced vertices in proton-proton collisions at  $\sqrt{s} = 13\text{ TeV}$ ”

[55]: Shuve et al. (2016), “Revision of the LHCb Limit on Majorana Neutrinos”

[56]: Aaij et al. (2021), “Search for heavy neutral leptons in  $W^+ \rightarrow \mu^+ \mu^\pm \text{jet}$  decays”

$|U_{\tau 4}|^2$ , where the latter is place the most stringent limits from  $10^{-3}$  to  $10^{-6}$  in the 0.1 GeV to 2 GeV range [39, 52, 53]. In Figure 1.4 the current strongest bounds on  $|U_{\tau 4}|^2$  are shown.

### Collider Searches

So far, collider searches have been conducted at the *large electron positron collider (LEP)* and at the *large hadron collider (LHC)* in proton-proton mode. Strongest results are from the ATLAS and CMS experiments, which are nearly hermetic, general purpose detectors around the interaction point, and from the DELPHI and the LHCb experiments, which are forward detectors that can be used to search for new particles in decays of heavy particles produced. In the minimal model, HNLs in the GeV mass range can be produced through mass mixing in decays of heavy mesons, tau leptons, Z/W bosons, H bosons, or top quarks originating from the collisions. Depending on the dirac or majorana nature of the HNL, they can decay to lepton number conserving or lepton number violating channels.

Using prompt and displaced decays of the HNL, both ATLAS and CMS have set constraints on  $|U_{e 4}|^2$  and  $|U_{\mu 4}|^2$  at the level of  $10^{-4}$  to  $10^{-6}$  in the mass range between 1 GeV to 100 GeV [41–44]. The LHCb experiment has HNL search results at HNL masses below and above the W boson mass, where the low mass searches are using the decay channel  $B^- \rightarrow \pi^+ \mu^- \mu^-$ , setting limits at the  $10^{-3}$  level for  $|U_{\mu 4}|^2$  in the mass range of 0.5 GeV to 3.5 GeV [55]. At high masses, the  $W^+ \rightarrow \mu^- \mu^\pm \text{jet}$  channel is used to set limits at the order of  $10^{-3}$  to  $10^{-2}$  for  $|U_{\mu 4}|^2$  in the mass range of 5 GeV to 50 GeV in the LNC channel and at the order of  $10^{-4}$  to  $10^{-3}$  in the LNV channel [56].

### Nuclear Decays Measurements

A novel approach of searching for irregularities in energy-momentum conservation measurements in nuclear reactions might be a viable way of

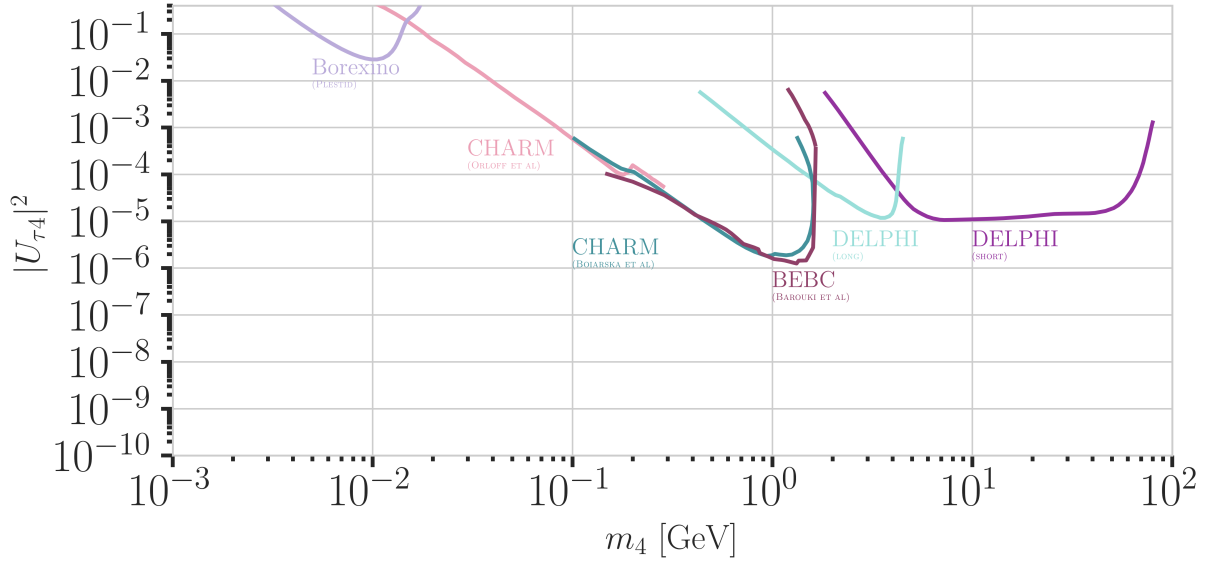


Figure 1.4: Current leading  $|U_{\tau 4}|^2 - m_4$  limits from BOREXINO [57], CHARM [52, 53], DELPHI [38], and BEBC [39]. Modified from [46].

searching for HNLs, as they could be interpreted as constraints on  $|U_{e4}|^2$  and  $m_4$ .

Kinks in **beta decay** spectra would show up at  $Q - m_4 c^2$ , where the HNL mass,  $m_4$ , can be measured between the lower energy detection threshold and the energy released in the decay, which is called  $Q$  value. Analyses using the tritium decay, with  $Q = 18.6$  keV, are planned in *KATRIN* [58] and *TRISTAN* [59] in the 1 keV to 18 keV range. Their projected statistical limits are around  $10^{-7}$  for  $|U_{e4}|^2$ , but will require further detector upgrades [59]. A first result from KATRIN measurements during commissioning sets limits at the order of  $10^{-2}$  to  $10^{-3}$  in the mass range of 0.1 keV to 1.6 keV [60]. *DUNE* is planning to measure the ionization charge of atmospheric argon decays, with  $Q = 565$  keV, to probe  $|U_{e4}|^2$  at in the 20 keV to 450 keV mass range. The projected sensitivity is at the  $10^{-5}$  level, and might improve to  $10^{-7}$  with additional detector improvements [61].

To test for the existence of HNLs using **electron capture** measurements, total energy-momentum reconstruction of all non-neutrino final states is needed. Electron capture is a pure two body decay process, where the recoiling atom and the electron neutrino are the only final state particles, but additional energy is carried away by the de-excitation x-ray or auger electron. The energy-momentum conservation can be probed by measuring the atom and the associated de-excitation products. The mixing  $|U_{e4}|^2$  can be probed by looking for a separated non-zero missing mass peak. The *BeEST* experiment has set limits at the  $10^{-4}$  level in the 100 keV to 850 keV mass range, using berillium-7, which has a  $Q$  value of 862 keV. After planned upgrades to the experiment, the sensitivity is expected to improve to the  $10^{-7}$  level [62].

**Reactor searches** up to 12 MeV in mass are possible at short baseline experiments using commercial or research reactors, which are a strong source of electron antineutrinos and could therefore also produce HNLs if  $|U_{e4}|^2$  is non-zero. Visible decay channels at these energies are  $\nu_4 \rightarrow \nu_e e^+ e^-$ ,  $\nu_4 \rightarrow \nu \gamma$ , and  $\nu_4 \rightarrow \nu \gamma \gamma$ , where the first dominates. The first analysis in this field, reports limits at the  $10^{-4}$  level in the 2 MeV to 7 MeV mass range [63].

mention the Z boson decay results from DELPHI (because they are strong in  $U_{\tau 4}$ , too (RED))

[58]: Osipowicz et al. (2001), “KATRIN: A Next generation tritium beta decay experiment with sub-eV sensitivity for the electron neutrino mass. Letter of intent”

[59]: Mertens et al. (2019), “A novel detector system for KATRIN to search for keV-scale sterile neutrinos”

[60]: Aker et al. (2023), “Search for keV-scale sterile neutrinos with the first KATRIN data”

[61]: Abi et al. (2020), “Deep Underground Neutrino Experiment (DUNE), Far Detector Technical Design Report, Volume II: DUNE Physics”

[62]: Friedrich et al. (2021), “Limits on the Existence of sub-MeV Sterile Neutrinos from the Decay of  $^7\text{Be}$  in Superconducting Quantum Sensors”

[63]: Hagner et al. (1995), “Experimental search for the neutrino decay  $\nu_3 + \nu_j + e^+ + e^-$  and limits on neutrino mixing”

## Atmospheric and Solar

Natural sources of neutrinos are provided up to 20 MeV by the sun and up to 100s of GeV by neutrino production in the atmosphere. Both fluxes contain all flavors of neutrinos, due to mixing and oscillations, and can therefore be used to directly probe the mixings with  $\nu_e$ ,  $\nu_\mu$ , and  $\nu_\tau$ . Depending on the HNL mass and the strength of the mixing, which both govern the decay length, different signatures can be used to experimentally access large regions of the HNL parameter space. The strength of the mixing defines the total rate of HNL events, which is additionally affected by whether solely the minimal mass mixing is assumed, or also more complicated mixing scenarios, like the dipole portal, are considered.

So far, only very few analyses exist, which are performed by the experimental collaborations themselves. Several external theoretical groups have predicted the expected sensitivities to HNLs, produced from solar or atmospheric neutrinos, based on various coupling scenarios and decay lengths. A selection of the potential analyses will be discussed in the following.

[34]: Bellini et al. (2013), “New limits on heavy sterile neutrino mixing in B8 decay obtained with the Borexino detector”

For very long-lived particles, **production inside the sun** can be used as a source to search for HNLs in detectors on earth. This will only allow production through non-zero  $|U_{e4}|^2$ , because the initial solar neutrino flux is only  $\nu_e$ . By searching for HNL decays to a SM neutrino and an electron positron pair  $\nu_4 \rightarrow \nu_e e^+ e^-$  and comparing to the expected inter planetary positron flux, *Borexino* has placed the strongest limits on the mixing  $|U_{e4}|^2$  at the order of  $10^{-5}$  in the few MeV mass range [34].

[57]: Plestid (2021), “Luminous solar neutrinos I: Dipole portals”

[64]: Plestid (2021), “Luminous solar neutrinos II: Mass-mixing portals”

For HNL decay length scales of the order of the Earth’s diameter, HNL **up-scattering outside the detector** is possible, where a neutrino from the solar or the atmospheric neutrino flux scatters in the Earth and transfers some kinetic energy into the mass of the HNL, which can then later decay inside the detector. For HNL masses below 18 MeV produced from solar neutrinos, (external) limits were derived using the Borexino data for purely tau coupling through mass mixing [57] and for all flavor coupling through the dipole portal [64]. At similar decay length scales, the HNL could also be produced directly in the atmosphere, but neither this channel, nor the production anywhere in the Earth from atmospheric neutrinos has been investigated yet.

[65]: Coloma et al. (2017), “Double-Cascade Events from New Physics in Icecube”

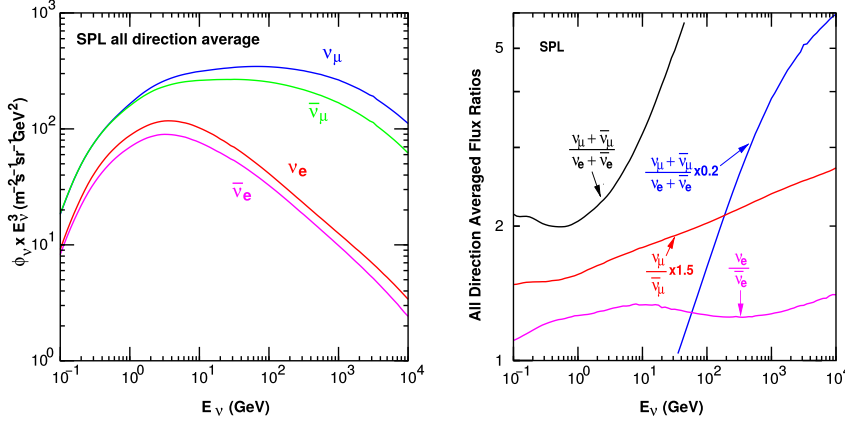
[66]: Coloma (2019), “Icecube/Deep-Core tests for novel explanations of the MiniBooNE anomaly”

[67]: Atkinson et al. (2022), “Heavy Neutrino Searches through Double-Bang Events at Super-Kamiokande, DUNE, and Hyper-Kamiokande”

[68]: Coloma et al. (2021), “GeV-scale neutrinos: interactions with mesons and DUNE sensitivity”

If the HNL decay lengths are sufficiently short, **production and decay in the detector** can happen and the observation of two vertices could be used to constrain the mixing parameters. In principle, this could be possible with any neutrino flavor produced in the sun or the atmosphere, but so far only theoretical studies have been performed for mass-mixing and dipole-portal couplings for the atmospheric neutrino detectors *IceCube* [65, 66] and *Super-K*, *Hyper-K*, and *Dune* [67, 68]. Due to the high complexity of these experiments, several simplified assumptions were made in the studies, which might not hold in reality, and the results should be taken with caution. For reliable sensitivity estimates and limits the collaborations should perform their own analyses.





**Figure 1.5:** The atmospheric fluxes of different neutrino flavors as a function of energy (left) and the ratios between muon neutrinos and electron neutrinos as well as the ratios between neutrinos and antineutrinos for both those flavors (right). Results from the calculations performed for the geographic South Pole, taken from [70].

## 1.3 Atmospheric Neutrinos as Source of Heavy Neutral Leptons

This work focuses on the search for HNLs using atmospheric neutrinos as source for the production and decay inside the IceCube detector. The following sections will give a brief overview of the production of neutrinos in the atmosphere and the oscillations they undergo, before discussing the expected signatures of HNLs in the detector, where they are produced from the incoming neutrinos and subsequently decay.

### 1.3.1 Production of Neutrinos in the Atmosphere

The analysis performed in this work is based on the sample of neutrinos observed in IceCube DeepCore at energies below 100 GeV. At these energies, the flux exclusively originates in the Earth's atmosphere. Highly relativistic cosmic rays (protons and heavier nuclei [69]) interact in the upper atmosphere, producing showers of secondary particles. Neutrinos are produced in decays of charged pions and kaons ( $\pi$  and  $K$  mesons) present in those showers, where the dominant contribution comes from the decay chain

$$\begin{aligned}\pi^\pm &\rightarrow \mu^\pm + \nu_\mu(\bar{\nu}_\mu), \\ \mu^\pm &\rightarrow e^\pm + \bar{\nu}_\mu(\nu_\mu) + \nu_e(\bar{\nu}_e),\end{aligned}\tag{1.22}$$

where muon neutrinos  $\nu_\mu$  and muons  $\mu^\pm$  are produced in the first decay and both electron and muon neutrinos  $\nu_{e/\mu}$  are produced in the second decay. Atmospheric muons, which are also produced in these decays, are the main background component for IceCube DeepCore analyses.

The different atmospheric flux components are shown in Figure 1.5 (left), for a much broader energy range than relevant for this work. Both neutrinos and antineutrino fluxes are shown for electron and muon neutrinos and all fluxes are the directionally averaged expectation calculated at the South Pole. Muon neutrinos are dominating the flux and from Equation 1.22 the naive assumption would be that the ratio between muon and electron neutrinos is  $(\nu_\mu + \bar{\nu}_\mu)/(\nu_e + \bar{\nu}_e) = 2$ . This is roughly true at energies below 1 GeV, where all muons decay in flight, but at larger energies muons can reach the detector before decaying, which increases the ratio to approximately 10:1 at around 100 GeV. Additionally, kaon decays start to contribute which also increases the number of muons and muon neutrinos. The increasing ratio can be seen

[69]: Tanabashi et al. (2018), "Review of Particle Physics"

in Figure 1.5 (right), which also shows the ration between neutrinos and antineutrinos for both flavors.

Charged mesons or tau particles can also be produced in cosmic ray interactions. Their decays lead to the production of tau neutrinos. At the energies relevant for this work however, the resulting tau neutrino flux is negligible as compared to the muon neutrino flux [71] and is not considered in the analysis. This is because both charged mesons and tau particles are much heavier than pions and kaons and therefore their production is suppressed at high energies.

[71]: Fedynitch et al. (2015), “Calculation of conventional and prompt lepton fluxes at very high energy”

Say something about atmospheric neutrino flux uncertainties, based on recent JP/Anatoli papers. (YELLOW)

### 1.3.2 Neutrino Oscillations

Describing neutrinos in their mass state as introduced in Section ?? is crucial to understand their propagation through space and time and to explain neutrino oscillations. Oscillations mean that a neutrino changes from its initial flavor, that it was produced with, to another flavor and back after traveling a certain distance.

The neutrino propagation in vacuum can be expressed by applying a plane wave approach, where the mass eigenstates evolve as

$$|v_k(t)\rangle = e^{-iE_k t/\hbar} |v_k\rangle . \quad (1.23)$$

The energy of the mass eigenstate  $|v_k\rangle$  is  $E_k = \sqrt{\vec{p}^2 c^2 + m_k^2 c^4}$ , with momentum  $\vec{p}$  and mass  $m_k$ ,  $\hbar$  is the reduced Planck constant, and  $c$  is the speed of light in vacuum. A neutrino is produced as a flavor eigenstate  $|v_\alpha\rangle$  in a CC weak interaction, but its propagation happens as the individual mass states it is composed of. The probability of finding the neutrino with initial flavor  $|v_\alpha\rangle$  in the flavor state  $|v_\beta\rangle$  after the time  $t$  is calculated as

$$P_{v_\alpha \rightarrow v_\beta}(t) = |\langle v_\beta | v_\alpha(t) \rangle|^2 , \quad (1.24)$$

[72]: Dirac (1927), “The Quantum Theory of the Emission and Absorption of Radiation”

by applying Fermi’s Golden Rule [72], which defines the transition rate from one eigenstate to another by the strength of the coupling between them. This coupling strength is the square of the matrix element and using the fact that the mixing matrix is unitary ( $U^{-1} = U^\dagger$ ) to describe the mass eigenstates as flavor eigenstates, we find the time evolution of the flavor state  $|v_\alpha(t)\rangle$ , which can be inserted into Equation 1.24 to find the probability as

$$P_{v_\alpha \rightarrow v_\beta}(t) = \sum_{j,k} U_{\beta j}^* U_{\alpha j} U_{\beta k} U_{\alpha k}^* e^{-i(E_k - E_j)t/\hbar} . \quad (1.25)$$

The indices  $j$  and  $k$  run over the mass eigenstates.

We can approximate the energy as

$$E_k \approx E + \frac{c^4 m_k^2}{2E} \longrightarrow E_k - E_j \approx \frac{c^4 \Delta m_{kj}^2}{2E} , \quad (1.26)$$

for small neutrino masses compared to their kinetic energy. Here,  $\Delta m_{kj}^2 = m_k^2 - m_j^2$  is the mass-squared splitting between states  $k$  and  $j$ . Replacing the time in Equation 1.25 by the distance traveled by relativistic neutrinos

$t \approx L/c$  we get

$$P_{\nu_\alpha \rightarrow \nu_\beta}(t) = \delta_{\alpha\beta} - 4 \sum_{j>k} \text{Re}(U_{\beta j}^* U_{\alpha j} U_{\beta k} U_{\alpha k}^*) \sin^2\left(\frac{c^3 \Delta m_{kj}^2}{4E\hbar} L\right) + 2 \sum_{j>k} \text{Im}(U_{\beta j}^* U_{\alpha j} U_{\beta k} U_{\alpha k}^*) \sin^2\left(\frac{c^3 \Delta m_{kj}^2}{4E\hbar} L\right), \quad (1.27)$$

which is called the survival probability if  $\alpha = \beta$ , and the transition probability if  $\alpha \neq \beta$ . Once again, this probability is only non-zero if there are neutrino mass eigenstates with masses greater than zero. Additionally, there must be a mass-squared difference  $\Delta m^2$  and non-zero mixing between the states. Since we assumed propagation in vacuum in Equation 1.23, the transition and survival probabilities correspond to vacuum mixing.

The mixing matrix can be parameterized as [69]

$$U = \begin{pmatrix} 1 & 0 & 0 \\ 0 & c_{23} & s_{23} \\ 0 & -s_{23} & c_{23} \end{pmatrix} \begin{pmatrix} c_{13} & 0 & s_{13}e^{-i\delta_{CP}} \\ 0 & 1 & 0 \\ -s_{13}e^{i\delta_{CP}} & 0 & c_{13} \end{pmatrix} \begin{pmatrix} c_{12} & s_{12} & 0 \\ -s_{12} & c_{12} & 0 \\ 0 & 0 & 1 \end{pmatrix}, \quad (1.28)$$

where  $c_{ij} = \cos \theta_{ij}$  and  $s_{ij} = \sin \theta_{ij}$  are cosine and sine of the mixing angle  $\theta_{ij}$ , that defines the strength of the mixing between the mass eigenstates  $i$  and  $j$ , and  $\delta_{CP}$  is the neutrino CP-violating phase. Experiments are sensitive to different mixing parameters, depending on the observed energy range, neutrino flavor, and the distance between the source and the detector  $L$ , commonly referred to as *baseline*. To be able to resolve oscillations the argument

$$\frac{\Delta m^2 L}{4E} \quad (1.29)$$

should be at the order of 1. This divides experiments into ones that are sensitive to very slow oscillations from  $\Delta m_{21}^2 \approx \mathcal{O}(10^{-5} \text{eV}^2)$  and ones that are sensitive to faster oscillations from  $\Delta m_{31}^2 \approx \mathcal{O}(10^{-3} \text{eV}^2)$ . Relevant for this work are the parameters that can be measured at the earth's surface using atmospheric neutrinos, which are  $\Delta m_{31}^2$ ,  $\theta_{23}$ , and  $\theta_{13}$ , because the flux is primarily composed of muon neutrinos and antineutrinos. Applying the parameterization from Equation 1.28 to Equation 1.27 and using the fact that  $\theta_{13}$  is small and  $\theta_{12}$  is close to  $\pi/4$ , the survival probability of muon neutrinos can be approximated as

$$P_{\nu_\mu \rightarrow \nu_\mu} \simeq 1 - 4|U_{\mu 3}|^2(1 - |U_{\mu 3}|^2) \sin^2\left(\frac{\Delta m_{31}^2 L}{4E}\right) \simeq 1 - \sin^2(2\theta_{23}) \sin^2\left(\frac{\Delta m_{31}^2 L}{4E}\right), \quad (1.30)$$

while the tau neutrino appearance probability is

$$P_{\nu_\mu \rightarrow \nu_\tau} \simeq 4|U_{\mu 3}|^2|U_{\tau 3}|^2 \sin^2\left(\frac{\Delta m_{31}^2 L}{4E}\right) \simeq \sin^2(2\theta_{23}) \sin^2\left(\frac{\Delta m_{31}^2 L}{4E}\right). \quad (1.31)$$

The latest global fit [73] of all the parameters is shown in Table 1.2.

[69]: Tanabashi et al. (2018), "Review of Particle Physics"

Parameter	Global Fit
$\theta_{12}$ [°]	$33.41^{+0.75}_{-0.72}$
$\theta_{13}$ [°]	$8.54^{+0.11}_{-0.12}$
$\theta_{23}$ [°]	$49.1^{+1.0}_{-1.3}$
$\Delta m_{21}^2$ [ $10^{-5} \text{eV}^2$ ]	$7.41^{+0.21}_{-0.20}$
$\Delta m_{31}^2$ [ $10^{-3} \text{eV}^2$ ]	$2.511^{+0.028}_{-0.027}$
$\delta_{CP}$ [°]	$197^{+42}_{-25}$

**Table 1.2:** Results from the latest global fit of neutrino mixing parameters from [73].

[73]: Esteban et al. (2020), "The fate of hints: updated global analysis of three-flavor neutrino oscillations"

say something about matter effect? (ORANGE)

say something about mass ordering? (ORANGE)

### 1.3.3 Neutrino Interactions with Nuclei

The neutrino detection principle of IceCube DeepCore is explained in Chapter 2 and relies on the weak interaction processes between neutrinos and the nuclei of the Antarctic glacial ice. At neutrino energies above 5 GeV, the cross-sections are dominated by *deep inelastic scattering (DIS)*, where the neutrino is energetic enough to resolve the underlying structure of the nucleons and interact with one of the composing quarks individually. As a result the nucleon breaks and a shower of hadronic secondary particles is produced. Depending on the type of interaction, the neutrino either remains in the final state for NC interactions or is converted into its charged lepton counterpart for CC interactions. The CC DIS interactions have the form

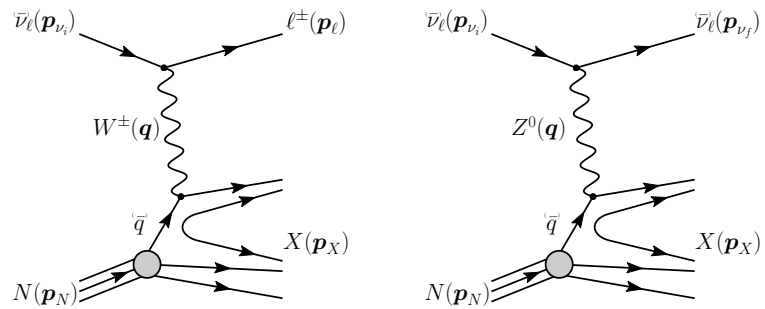
$$\begin{aligned} \nu_l + N &\rightarrow l^- + X, \\ \bar{\nu}_l + N &\rightarrow l^+ + X, \end{aligned} \quad (1.32)$$

where  $\nu_l/\bar{\nu}_l$  and  $l^-/l^+$  are the neutrino/antineutrino and its corresponding lepton/antilepton, and  $l$  can be either an electron, muon, or tau.  $N$  is the nucleon and  $X$  stands for any set of final state hadrons. The NC DIS interactions are

$$\begin{aligned} \nu_l + N &\rightarrow \nu_l + X \text{ and} \\ \bar{\nu}_l + N &\rightarrow \bar{\nu}_l + X. \end{aligned} \quad (1.33)$$

Figure 1.6 shows the Feynman diagrams for both processes DIS interactions

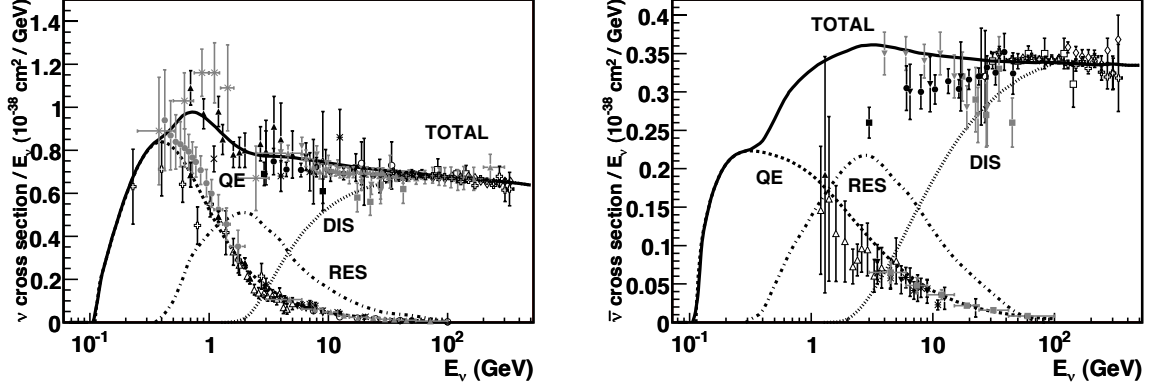
**Figure 1.6:** Feynman diagrams for deep inelastic scattering of a neutrino with a nucleon via charged-current (left) and neutral current (right) interactions.  $p_{\nu_i}$ ,  $p_N$  and  $p_{\nu_f}$ ,  $p_l$ ,  $p_N$  are the input and output four-momenta, while  $q$  is the momentum transfer. Taken from [74].



have a roughly linear energy dependent cross-section above  $\sim 20$  GeV and are well measured and easy to theoretically calculate. They are the primary interaction channel for neutrinos detected with IceCube.

At energies below 5 GeV, *quasi-elastic scattering (QE)* and *resonant scattering (RES)* become important. At these energies the neutrinos interact with the approximately point-like nucleons, without breaking them up in the process. RES describes the process of a neutrino scattering off a nucleon producing an excited state of the nucleon in addition to a charged lepton. It is the dominant process at 1.5 GeV to 5 GeV for neutrinos and 1.5 GeV to 8 GeV for antineutrinos. Below 1.5 GeV QE is the main process, where protons are converted to neutrons in antineutrino interactions and vice-versa for neutrino interactions. Additionally, a charged lepton corresponding to the neutrino/antineutrino flavor is produced. The cross-sections of QE and RES scattering processes are not linear in energy and the transition region from QE/RES to DIS is poorly understood. The total cross-sections and their composition is shown in Figure 1.7. It can be seen that the interaction cross-sections are very small at the order of  $10^{-38} \text{ cm}^2$ . This is the reason why very

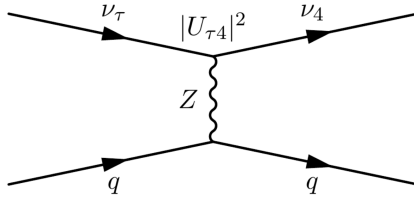
large volume detectors are required to measure atmospheric neutrinos with sufficient statistics to perform precision measurements of their properties. The interaction length of a neutrino with  $E_\nu = 10$  GeV is of  $\mathcal{O}(10 \times 10^{10} \text{ km})$ , for example.



**Figure 1.7:** Total neutrino (left) and antineutrino (right) per nucleon cross-section divided by neutrino energy plotted against energy. The three main scattering processes quasi-elastic scattering (QE), resonant scattering (RES), and deep-inelastic scattering (DIS) are shown. Taken from [75].

### 1.3.4 Heavy Neutral Lepton Production and Decay

For the search conducted in this work, both production and decay are assumed to happen inside the detector, therefore probing decay lengths ranges at the scale of the detector size, which is below 1000 m. Since the mixing with the first two generations of leptons is already strongly constrained as was discussed in Section 1.3, only the mixing with the tau neutrino will be considered in the following. Due to the effect of oscillations, described in Section 1.3.2, the initial atmospheric muon neutrino flux provides a sizable tau neutrino flux at the detector.

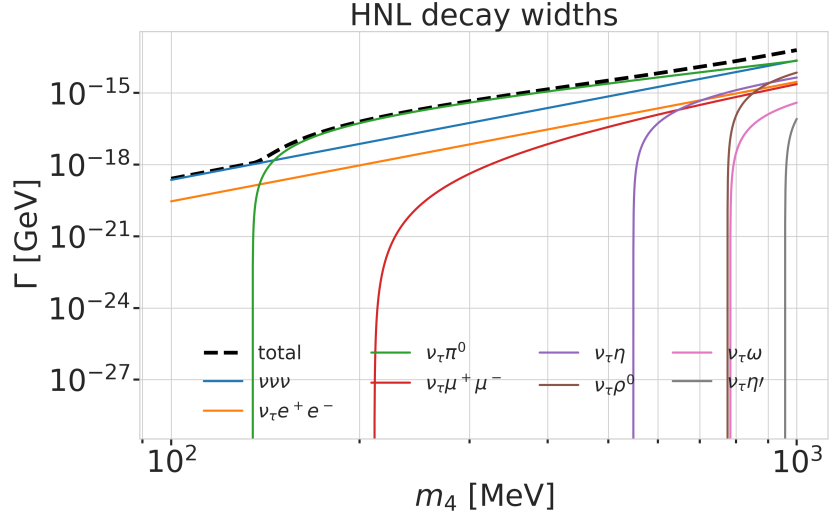


**Figure 1.8:** Feynman diagram of the HNL production. The heavy mass state is produced in the up-scattering of a tau neutrino.

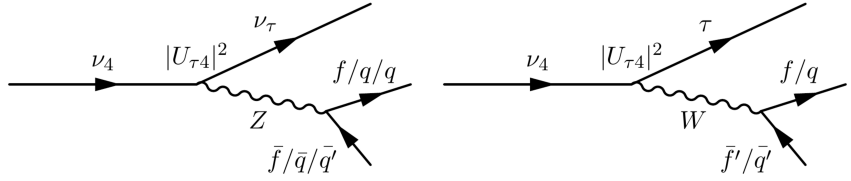
For a non-zero  $|U_{\tau 4}|^2$ , the HNL can be produced through **up-scattering in the ice**. An incoming tau neutrinos scatters on an ice nucleus and transfers some of its kinetic energy to the heavy neutrino. The Feynman diagram of this process is shown in Figure 1.8. The custom NC cross-sections calculated for this purpose are explained in more detail in Section ??, but are similar to the SM tau neutrino NC cross-sections, with a reduction scaling with the mixing  $|U_{\tau 4}|^2$  and energy dependent reductions, due to kinematic constraints because of the heavy neutrino mass. The scattering process produces a hadronic cascade, which will produce light in the detector.

After a certain distance, the HNL will **decay in the ice**, where the possible decay channels considered in this work are shown in Figure 1.9 and the underlying, explicit calculations are discussed in Section ?. The decay can be a CC or NC and both purely leptonic and leptonic+mesonic modes

**Figure 1.9:** Decay widths of the HNL within the mass range considered, calculated based on the results from [68]. Given the existing constraints on  $|U_{e4}|^2$  and  $|U_{\mu 4}|^2$ , we consider that the corresponding decay modes are negligible.



**Figure 1.10:** Feynman diagram of the HNL decay. The heavy mass state can decay through neutral current interaction (left) into a tau neutrino and a charged lepton or quark pair, or through charged current interaction (right) into a tau lepton and a charged lepton or quark.



are possible. The Feynman diagrams of the decays can be seen in Section ?? . Only the mass range relevant for this work is presented and mixing with  $\nu_{e/\mu}$  is assumed to be negligible. Depending on the decay channel, an electromagnetic or a hadronic cascade is produced, while some energy is carried away by the invisible neutrino. The decay length of the HNL is defined by its proper lifetime<sup>1</sup>, which is given by

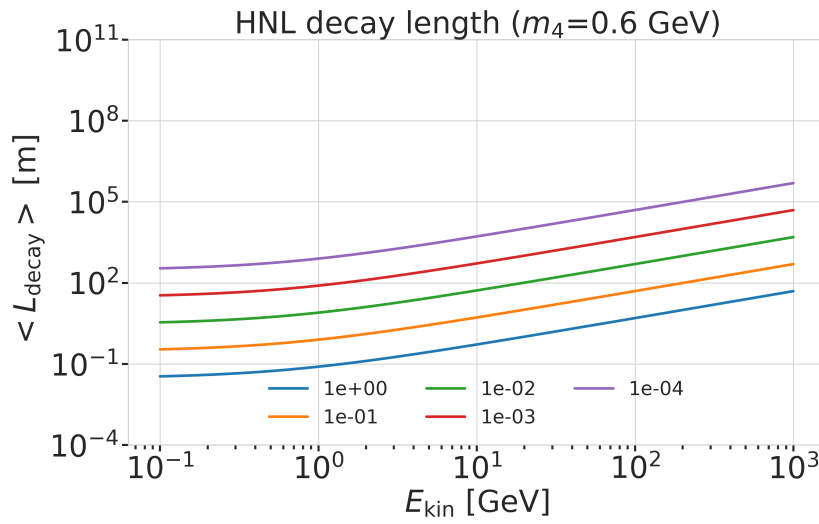
$$\tau_{\text{proper}} = \frac{\hbar}{\Gamma_{\text{total}}(m_4) \cdot |U_{\tau 4}|^2}, \quad (1.34)$$

where  $\hbar$  is the reduced Planck constant,  $\Gamma_{\text{total}}(m_4)$  is the total decay width of the HNL for the given mass, and  $|U_{\tau 4}|^2$  is the mixing with the tau neutrino. The total decay width is the sum of the partial decay widths for all possible decay channels. The mean lab frame decay length is then given by

$$L_{\text{decay}} = \gamma v \tau_{\text{proper}}, \quad (1.35)$$

where  $\gamma$  is the Lorentz factor of the HNL, defined by the kinetic energy. This will be further discussed on Section ?? . Figure 1.11 shows the mean decay lengths for an example mass of  $m_4 = 0.6 \text{ GeV}$  and several mixing values.

1: A particle decay time follows an exponential distribution, with mean lifetime given by the proper lifetime. The proper lifetime is the lifetime in the rest frame of the particle.



**Figure 1.11:** Theoretical mean decay length of the HNL for a mass of 0.6 GeV and different mixing values.



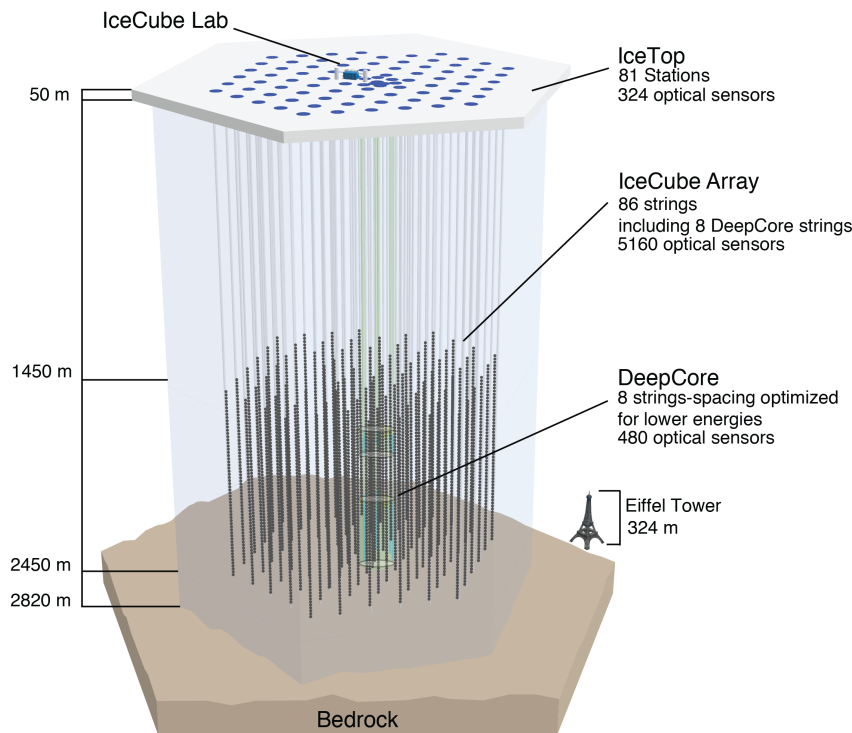


The IceCube Neutrino Observatory [76] is a cubic-kilometer, ice-Cherenkov detector located at the geographic South Pole. IceCube utilizes the Antarctic glacial ice as detector medium to observe neutrinos by measuring the Cherenkov light produced from secondary charged particles. It was deployed between 2006 and 2011 and has been taking data since the installation of the first modules. The primary goal of IceCube is the observation of astrophysical neutrinos as a telescope, but it can also be used to study fundamental particle physics properties using the same astrophysical neutrinos, and by measuring atmospheric neutrinos as well as studying cosmic rays.

This chapter first describes the detector and its subcomponents in Section 2.1, the propagation of particles through ice is explained in Section 2.2, and finally, the signatures that IceCube can observe of the different particles are introduced in Section 2.3.

2.1	Detector Components	19
2.2	Particle Propagation in Ice	22
2.3	Event Morphologies	25

## 2.1 Detector Components



[76]: Aartsen et al. (2017), “The IceCube Neutrino Observatory: instrumentation and online systems”

**Figure 2.1:** Overview of the IceCube detector showing the in-ice main- and sub-array IceCube and DeepCore, IceTop, and the IceCube Laboratory. From [76].

The full IceCube detector array consists of 86 vertical, in-ice strings and 81 surface stations as shown in Figure 2.1. The in-ice part is composed of 60 optical modules per string deployed at depths of 1450 m - 2450 m below the ice, while the surface stations of the cosmic air-shower array, *IceTop*, are ice-filled tanks. The surface stations and the majority of the strings are arranged in a hexagonal grid with the operations building, the *IceCube Laboratory* (ICL), central to the grid on the surface. A top view of the hexagonal arrangement

is shown in Figure 2.4. The in-ice array is designed to detect neutrinos in the energy range from GeV to PeV.

### 2.1.1 Digital Optical Modules and the Antarctic Ice

The IceCube detection medium is the Antarctic glacial ice itself, which was formed over 100 000 years by accumulation of snow that was subsequently compressed by its own weight to form a dense crystal structure [77]. As a result of this formation process, the optical properties, scattering and absorption, primarily change with depth. Within the detector volume the absorption length ranges from 100 m - 400 m, while the scattering length lies between 20 m and 100 m. They are correlated, with the absorption length being roughly four times the scattering length [78]. The vertical distribution of the absorption length can be seen in Figure 2.2, where one dominant feature is the *dust layer* between 2000 m and 2100 m depth. This region has a higher concentration of dust particles that were deposited in a period of high volcanic activity, which leads to bad optical properties in form of larger scattering and absorption.

[77]: Price et al. (2000), "Age vs depth of glacial ice at South Pole"

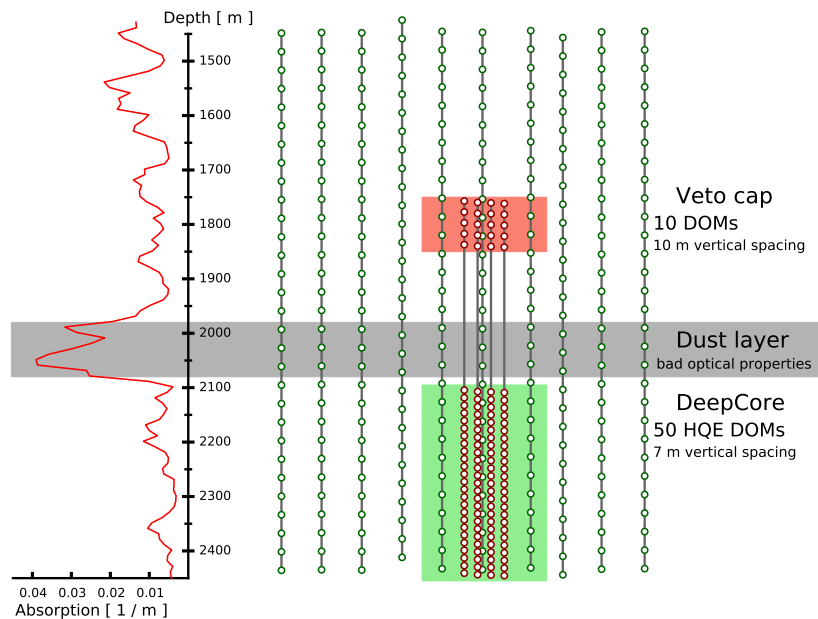
SB: there are more properties than just these. Somehow need a half sentence that explains why these are particularly important to single out (see ice papers for inspiration) (RED)

CL: maybe define what absorption and scattering lengths are? they are defined differently so this invites a comparison that is not so obvious (RED)

[78]: Abbasi et al. (2022), "In-situ estimation of ice crystal properties at the South Pole using LED calibration data from the IceCube Neutrino Observatory"

Add reference for the dust layer! Maybe also from the ice paper? mention/cite dust logger paper/procedure? (RED)

**Figure 2.2:** Side view of IceCube and DeepCore showing the depth dependent scattering and absorption length (left panel) and the DOM positions around the dust layer.

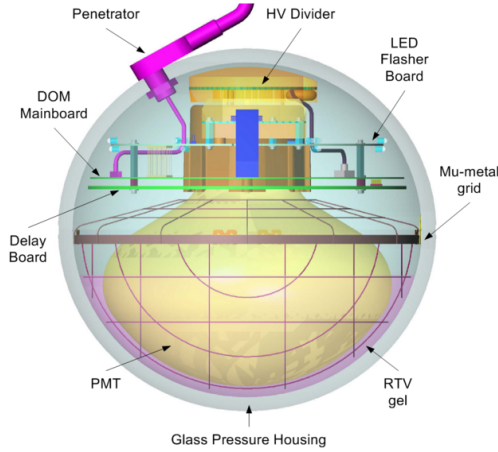


[79]: Abbasi et al. (2009), "The IceCube data acquisition system: Signal capture, digitization, and timestamping"

[79]: Abbasi et al. (2009), "The IceCube data acquisition system: Signal capture, digitization, and timestamping"

The ice is instrumented by 5160 optical sensors called *digital optical modules* (DOMs) [79], which can detect the Cherenkov light produced by charged particles traveling through the ice. Each DOM is made of a spherical glass housing, containing a downward-facing *photomultiplier tube* (PMT), the main-board with control, readout, and processing-electronics, and a LED flasher-board for calibration purposes. The design and the individual components of a DOM can be seen in Figure 2.3.

The majority of PMTs are the 10" Hamamatsu R7081-02, which have a bialkali photocathode and are sensitive to wavelengths in the range of 300 nm to 650 nm, with a peak quantum efficiency of 25 % at 390 nm. The average dark count rate during operation in the ice is  $\sim 300$  Hz. The DOM electronics measure the PMT voltage and control the gain. At a voltage crossing of the equivalent to 0.25 PE the waveform readout is activated [79]. Only when either one of the nearest or next to nearest DOMs above or below also sees a



**Figure 2.3:** Design and components of a digital optical module (DOM) [79]

voltage crossing within a  $1\text{ }\mu\text{s}$  time window<sup>1</sup>, the voltages are digitized and sent to the ICL. Through the application of a waveform unfolding algorithm, called *WaveDeform* [80], the waveforms are compressed, and the results are the reconstructed times and charges of the photo-electrons. This is the basis for all further IceCube data processing.

The PMT is covered with a mu-metal grid (made from wire mesh), shielding the photocathode from Earth’s magnetic field, and it is optically coupled to the glass sphere by RTV silicone gel. The glass sphere is a pressure vessel, designed to withstand both the constant ice pressure and the temporary pressure during the refreezing process of the water in the drill hole during deployment (peaking at around 690 bar). The sphere is held by a harness that connects the DOMs along a string and also guides the cable for power supply and communication beside them.

The flasher-board controls 12 LEDs that produce optical pulses with a wavelength of 405 nm [76]. The LEDs can be pulsed separately or in combination with variable output levels and pulse lengths. Using the known information of the light source positions and times this can be used for in-situ calibration of the detector by measuring absorption and scattering properties of the ice. Calibrating the absolute efficiency of the DOMs itself is more accurately done using minimum ionizing muons [81, 82], since the total amplitude of the LED light is not well known.

### 2.1.2 IceCube Main-Array

The 78 strings that are arranged in a hexagonal pattern from the main part of the in-ice array, which is called *IceCube*. With a  $\sim 125\text{ m}$  horizontal spacing between the strings and a  $\sim 17\text{ m}$  vertical spacing between DOMs, IceCube has a lower energy threshold of around 100 GeV. IceCube was designed to detect high energy neutrinos of astrophysical origin.

The coordinate system that is used in IceCube is centered at 46500’E, 52200’N at an elevation of 883.9 m [76]. Per definition, it is a right-handed coordinate system where the y-axis points along the Prime Meridian (Grid North) towards Greenwich, UK, and the x-axis points 90° clockwise from the y-axis (Grid East). The z-axis is normal to the ice surface, pointing upwards. For IceCube analyses depth is defined as the distance along the z axis from the ice surface, fixed at an elevation of 2832 m.

1: This is referred to as a *hard local coincidence (HLC)* [79].

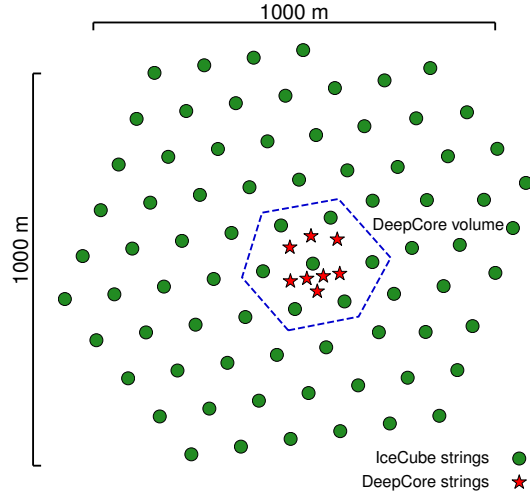
[80]: Aartsen et al. (2014), “Energy Reconstruction Methods in the IceCube Neutrino Telescope”

[76]: Aartsen et al. (2017), “The IceCube Neutrino Observatory: instrumentation and online systems”

[81]: Feintzeig (2014), “Searches for Point-like Sources of Astrophysical Neutrinos with the IceCube Neutrino Observatory”

[82]: Kulacz (2019), “In Situ Measurement of the IceCube DOM Efficiency Factor Using Atmospheric Minimum Ionizing Muons”

[76]: Aartsen et al. (2017), “The IceCube Neutrino Observatory: instrumentation and online systems”



**Figure 2.4:** Top view of the IceCube array.

### 2.1.3 DeepCore Sub-Array

[83]: Abbasi et al. (2012), “The design and performance of IceCube Deep-Core”

2: At 400 nm they are 35 % more efficient than the IceCube PMTs [83].

[83]: Abbasi et al. (2012), “The design and performance of IceCube Deep-Core”

The additional 8 strings form a denser sub-array of IceCube called *DeepCore* [83]. It is located at the bottom-center of the in-ice array and its *fiducial volume* also includes the 7 surrounding IceCube strings as shown in Figure 2.4. The strings in this region have a closer average horizontal distance of about 70 m. The lower 50 DeepCore DOMs on each string are placed in the region of clear ice below the dust layer between 2100 m to 2450 m depth, where their vertical spacing is  $\sim 7$  m. The remaining 10 modules on each string are placed above the dust layer to be used as veto against atmospheric muons as can be seen in Figure 2.2. Additionally, the DeepCore DOMs are equipped with higher quantum efficiency PMTs<sup>2</sup>. The combination of the denser spacing, the high quantum efficiency modules, and the most favorable ice properties below the dust layer leads to a lower energy detection threshold of around 5 GeV, allowing the more efficient observation of atmospheric neutrinos. This lower energy threshold enables measurements of neutrino oscillations and many other BSM studies such as dark matter, non-standard interactions, and sterile neutrinos [83].

## 2.2 Particle Propagation in Ice

Neutrinos interacting in the ice via DIS produce muons, electromagnetic showers, and hadronic showers, depending on their flavor and the interaction type. The particles produced in those processes mainly lose their energy through *ionization*, *bremsstrahlung*, *pair production*, and the *photo-nuclear interaction*. Electrically charged particles also emit Cherenkov light when traveling through the ice, which is the main observable in IceCube, but only contributes a small amount to the total energy loss. The Cherenkov effect and the energy losses of the particles are described in the following sections, followed by an overview of the different particle signatures in IceCube.

### 2.2.1 Cherenkov Effect

The detection principle of IceCube DeepCore is based on the observation of Cherenkov photons that are emitted by the charged secondary particles

produced in the neutrino interactions that were introduced in Section 1.3.3. The Cherenkov effect was first observed by Pavel Cherenkov in 1934 [84] and occurs when the charged particle travels faster than the phase velocity of light, therefore polarizing the medium. Upon de-excitation the molecules emit the received energy as photons in a spherical wavefront. Since the particle moves past this wavefront, the superposition of the spherical light emissions forms a cone, which is shown in blue in the bottom panel of Figure 2.5.

Using trigonometry, the angle  $\theta_c$  at which the Cherenkov light is emitted can be calculated as

$$\theta_c = \arccos\left(\frac{1}{\beta n}\right), \quad (2.1)$$

where  $\beta = v/c_{\text{vacuum}}$  is the velocity of the particle in units of the speed of light, and  $n$  is the refractive index of the medium that defines the speed of light in the medium  $c = c_{\text{vacuum}} \cdot n$ . When the particle velocity is close to the speed of light, the equation holds and the angle is only dependent on the refractive index of the medium. For the ice, the refractive index is  $n \approx 1.3$  and as a result  $\theta_c \approx 41^\circ$  [85].

The frequency of the emission depends on the charge  $z$  and the wavelength-dependent index of refraction  $n(\omega)$  and is given by the Frank-Tamm formula [86, 87]

$$\frac{d^2N}{dx d\lambda} = \frac{2\pi\alpha z^2}{\lambda^2} \left(1 - \frac{1}{\beta^2 n(\omega)^2}\right), \quad (2.2)$$

with  $\alpha \approx 1/137$  the fine structure constant,  $\lambda$  the wavelength of the emitted light, and  $x$  the path length traversed by the particle. Relativistic particles in ice produce roughly 250 photons per cm in the wavelength range of 300 nm - 500 nm [88].

## 2.2.2 Energy Losses

Even though relativistic, charged particles traveling through matter produce Cherenkov radiation, their energy is mainly lost through other processes that are dependent on the particle type and energy. The exact principles of energy loss for the different types can broadly be categorized into the three groups: quasi-continuous energy loss by muons, electromagnetic cascades, and hadronic cascades.

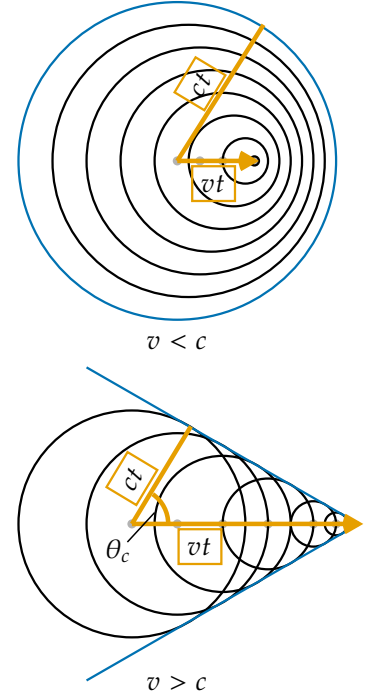
### Muons

Muons lose their energy by ionization, bremsstrahlung, pair production, and the photo-nuclear effect. The energy loss by ionization is the dominant process for muons above 1 GeV and has a weak energy dependence given by [15]

$$\left\langle -\frac{dE}{dx} \right\rangle = a_I(E) + b_R(E) \cdot E, \quad (2.3)$$

where  $E$  is the energy and  $a_I(E)$  and  $b_R(E) \cdot E$  are the energy loss by ionization and the combined radiative losses, respectively. In the energy range relevant for this work (10 GeV - 100 GeV), the parameters  $a_I$  and  $b_R$  only depend on

[84]: Cherenkov (1937), "Visible Radiation Produced by Electrons Moving in a Medium with Velocities Exceeding that of Light"



**Figure 2.5:** Schematic depiction of the spherical light front produced by a particle traveling slower than the speed of light in the medium (top) and the formation of the Cherenkov light front produced by a charged particle traveling faster than the speed of light in the medium (bottom). The speed of light in the medium is  $c$ ,  $v$  is the speed of the particle, and  $t$  is the time that has passed. Blue is the resulting wavefront, while the black circles are spherically emitted light at each position and the orange arrows show the direction of the particle.

[85]: Petrenko et al. (2002), "214Optical and electronic properties"

[86]: Frank et al. (1937), "Coherent visible radiation from fast electrons passing through matter"

[87]: Tamm (1991), "Radiation Emitted by Uniformly Moving Electrons"

[88]: Rädle et al. (2012), "Calculation of the Cherenkov light yield from low energetic secondary particles accompanying high-energy muons in ice and water with Geant4 simulations"

[15]: Workman et al. (2022), "Review of Particle Physics"



energy very weakly and can be approximated by constants. The energy loss is then given by

$$\left\langle -\frac{dE}{dx} \right\rangle = a + b \cdot E. \quad (2.4)$$

Based on this description, there is a critical energy which divides the regimes where ionization and radiative losses dominate. The critical energy is given by  $E_{\text{crit}} = a/b$  and for muons in ice it is  $\sim 713$  GeV (using  $a \approx 2.59 \text{ MeVcm}^{-1}$  and  $b \approx 3.63 \times 10^{-6} \text{ cm}^{-1}$  [89]). Since the energy range of interest is well below this critical energy, the range of a muon can easily be related to its energy by

$$\langle L \rangle = \frac{E_0}{a}. \quad (2.5)$$

Measuring the length of a muon track therefore allows for an estimation of its energy if the full track is contained within the instrumented volume of IceCube. Using the given numbers a 30 GeV muon travels  $\sim 116$  m, which is well within the instrumented volume of IceCube, which spans across distances of up to 1000 m. This approximate treatment does not take into account the stochastic nature of some energy losses. Bremsstrahlung and photo-nuclear interactions for example rarely occur, but when they do, they deposit a large chunk of energy. A thorough investigation of the energy losses of muons in ice can be found in [90].

## Electromagnetic Showers

Photons as well as electrons and positrons are produced either directly in neutrino interactions or in secondary particle interactions. Above a critical energy  $E_c$ , they lose their energy through repeated pair production and bremsstrahlung emission forming an expanding, electromagnetic shower profile. The particles' energy reduces with every interaction and their number increases until they fall below the critical energy where ionization and excitation of surrounding atoms become the dominant energy loss processes for electrons and positrons. For photons the remaining energy is lost through the Compton effect and the photoelectric effect [15]. Below the critical energy no new shower particles are produced.

Electromagnetic cascades can be characterized by the radiation length,  $X_0$ , after which electrons/positrons reduced their energy to  $1/e$  of their initial energy. For photons, it's equivalent to  $7/9$  of the mean free path of pair production. The critical energy for ice is  $E_c \approx 78$  MeV, with a radiation length of  $X_0 \approx 39.3$  cm [69].

The radiation length governs the longitudinal shower profile and using  $t = x/X_0$ , the shower intensity can be described by a gamma distribution [15, 91]

$$\frac{dE}{dt} = E_0 b \frac{(bt)^{a-1} e^{-bt}}{\Gamma(a)}, \quad (2.6)$$

where  $a$  and  $b$  are parameters that have to be estimated from experiment, and  $E_0$  is the initial shower energy. Based on the work from [90], performed with GEANT4 [92], the parameters for electromagnetic showers in ice are

$$e^- : a \approx 2.01 + 1.45 \log_{10}(E_0/\text{GeV}), b \approx 0.63, \quad (2.7a)$$

$$e^+ : a \approx 2.00 + 1.46 \log_{10}(E_0/\text{GeV}), b \approx 0.63, \quad (2.7b)$$

$$\gamma : a \approx 2.84 + 1.34 \log_{10}(E_0/\text{GeV}), b \approx 0.65. \quad (2.7c)$$

[89]: Chirkin et al. (2004), "Propagating leptons through matter with Muon Monte Carlo (MMC)"

[90]: Raedel (2012), "Simulation Studies of the Cherenkov Light Yield from Relativistic Particles in High-Energy Neutrino Telescopes with Geant4"

[15]: Workman et al. (2022), "Review of Particle Physics"

[69]: Tanabashi et al. (2018), "Review of Particle Physics"

[15]: Workman et al. (2022), "Review of Particle Physics"

[91]: Longo et al. (1975), "Monte Carlo Calculation of Photon Initiated Electromagnetic Showers in Lead Glass"

[90]: Raedel (2012), "Simulation Studies of the Cherenkov Light Yield from Relativistic Particles in High-Energy Neutrino Telescopes with Geant4"

[92]: Agostinelli et al. (2003), "Geant4—a simulation toolkit"

The maximum of the shower is at  $t_{max} = (a - 1)/b$  and the Cherenkov emission of the charged particles produced in the shower is peaked around the Cherenkov angle, since they are produced in the forward direction.

Add angular profile plot (Summer agrees!) (create one based on Leif R  del as Alex did) (RED)

### Hadronic Showers

In DIS interactions, a cascade is always produced by the hadrons coming from the target nucleus that is breaking apart. The cascade is a result of secondary particles produced in strong interactions between the hadrons and the traversed matter. The charged particles produced in the shower will emit Cherenkov radiation, while neutral particles will be invisible to the detector. There is also an electromagnetic component of the shower, for example, due to the decay of neutral pions into photons. Hadronic showers of the same energy as electromagnetic showers have larger fluctuations in energy deposition and shape, since they depend on the produced particle types. Hadrons also have a higher energy threshold for Cherenkov light production, because of their higher mass. Based on [90, 93], the visible electromagnetic fraction of hadronic showers can be parameterized as

$$F(E_0) = \frac{T_{\text{hadron}}}{T_{\text{EM}}} = 1 - (1 - f_0) \left( \frac{E_0}{E_s} \right)^{-m}, \quad (2.8)$$

where  $T_{\text{hadron/EM}}$  is the total track length of a hadronic/electromagnetic shower with the same energy,  $f_0$  is the ratio of hadronic and electromagnetic light yield,  $E_0$  is the initial energy, and  $E_s$  is an energy scale. The parameter  $m$  is a free model parameter. The ratio  $F(E_0)$  increases with energy, but is always smaller than 1. The variance of this distribution is given by

$$\sigma_F(E_0) = \sigma_0 \log(E_0)^{-\gamma}. \quad (2.9)$$

The parameters  $m$ ,  $E_s$ , and  $f_0$  were estimated by fitting the model to the results of Geant4 simulations. Cherenkov light from hadronic showers also peaks around the Cherenkov angle, but the angular distribution is more smeared out, due to the variations in particle type and their energy depositions.

[90]: Raedel (2012), "Simulation Studies of the Cherenkov Light Yield from Relativistic Particles in High-Energy Neutrino Telescopes with Geant4"  
 [93]: Gabriel et al. (1994), "Energy dependence of hadronic activity"


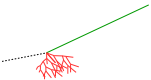

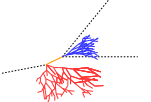
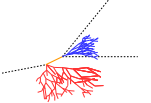
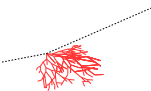
## 2.3 Event Morphologies

The event morphologies produced by particles detected in IceCube are combinations of the three energy loss types described in Section 2.2.2, e.g. *cascades* from electromagnetic and hadronic showers and elongated *tracks* from muons traveling through the detector. Table 2.1 gives an overview of the possible event signatures.

**Neutrino** interactions are observed as cascades, tracks, or a combination of both, depending on the initial flavor and the interaction type for the specific event.

In  $\nu_\mu$  - CC interactions, a muon is produced in addition to a hadronic shower from the breaking nucleus. If the interaction happens outside the detector, but the muon passes through the detector, this will create a track-like signature. The same happens if the interaction happens inside, but the

**Table 2.1:** IceCube low energy event signatures, their underlying interaction type, and the particles that produce them. Also shown are the secondary particles produced in the interactions. Black dashed lines represent neutrinos, green lines muons, orange line leptons, and blue and red lines are particles in electromagnetic and hadronic cascades, respectively. Adapted from [74].

Interaction	Secondary particles	Signature
$\text{CC } \nu_\mu^{(-)}$	 $\mu^\pm$ track	Track-only
$\text{CC } \nu_\mu^{(-)}$	 $\mu^\pm$ track and hadrons	Cascade + track
$\text{CC } \nu_\tau^{(-)}$	 $\tau^\pm$ decaying into $\mu^\pm$ (~17% BR), hadrons	Cascade + track
$\text{CC } \nu_\tau^{(-)}$	 $\tau^\pm$ decaying into $e^\pm$ or hadrons (~83% BR)	
$\text{CC } \nu_e^{(-)}$	 $e^\pm$ , hadrons	Cascade-only
$\text{NC } \nu_\ell^{(-)}$	 hadrons	

energy transfer to the nucleus is small ( $y \approx 0$ ). At energies relevant for this work, tracks have length at the same order of the distance between DOMs, so they can be observed as such.

If the interaction happens inside the detector and the energy transfer to the hadronic part of the shower is larger, it will create a cascade with a track leaving it. A similar signature is observed after a  $\nu_\tau$  - CC interaction, in which a tau is produced that later decays into a muon, with a branching ratio of 17 %. In those cases the muon usually has a lower energy and the track will be fainter and harder to observe.

The other 83 % of  $\nu_\tau$  - CC interactions produce a tau that decays into an electron or hadrons, leaving a cascade-only signature through the electromagnetic or hadronic shower. All  $\nu_e$  - CC interactions also produce pure cascades, since the electron quickly loses its energy in an electromagnetic shower. In all  $\nu$  - NC interactions, the produced neutrino escapes and only the hadronic shower is observable. Since the size of the cascades at the energy range of interest is smaller than the spacing of the DOMs, they are approximately observed as point-like, spherical light sources. This is just an approximation, though, and some asymmetry remains in the light profile, which can be used to reconstruct the direction of the incoming neutrino.

**Atmospheric muons** also produce pure track like signatures, similar to  $\nu_\mu$  - CC interactions happening outside the detector. They are one of the main backgrounds for analyses using atmospheric neutrinos and are therefore the target of many filter steps described in Section ??.



# Bibliography

Here are the references in citation order.

- [1] C. N. Yang and R. L. Mills. “Conservation of Isotopic Spin and Isotopic Gauge Invariance”. In: *Physical Review* 96.1 (Oct. 1954), pp. 191–195. doi: [10.1103/PhysRev.96.191](https://doi.org/10.1103/PhysRev.96.191) (cited on page 1).
- [2] S. Weinberg. “A Model of Leptons”. In: *Phys. Rev. Lett.* 19 (21 Nov. 1967), pp. 1264–1266. doi: [10.1103/PhysRevLett.19.1264](https://doi.org/10.1103/PhysRevLett.19.1264) (cited on page 1).
- [3] S. L. Glashow. “Partial-symmetries of weak interactions”. In: *Nuclear Physics* 22.4 (Feb. 1961), pp. 579–588. doi: [10.1016/0029-5582\(61\)90469-2](https://doi.org/10.1016/0029-5582(61)90469-2) (cited on page 1).
- [4] R. Jackiw. “Physical Formulations: Elementary Particle Theory. Relativistic Groups and Analyticity. Proceedings of the eighth Nobel Symposium, Aspenäsgråden, Lerum, Sweden, May 1968. Nils Svartholm, Ed. Interscience (Wiley), New York, and Almqvist and Wiksell, Stockholm, 1969. 400 pp., illus. \$31.75.” In: *Science* 168.3936 (1970), pp. 1196–1197. doi: [10.1126/science.168.3936.1196.b](https://doi.org/10.1126/science.168.3936.1196.b) (cited on page 1).
- [5] P. Higgs. “Broken symmetries, massless particles and gauge fields”. In: *Physics Letters* 12.2 (1964), pp. 132–133. doi: [https://doi.org/10.1016/0031-9163\(64\)91136-9](https://doi.org/10.1016/0031-9163(64)91136-9) (cited on page 1).
- [6] S. Chatrchyan et al. “Observation of a New Boson at a Mass of 125 GeV with the CMS Experiment at the LHC”. In: *Phys. Lett. B* 716 (2012), pp. 30–61. doi: [10.1016/j.physletb.2012.08.021](https://doi.org/10.1016/j.physletb.2012.08.021) (cited on page 1).
- [7] G. Aad et al. “Observation of a new particle in the search for the Standard Model Higgs boson with the ATLAS detector at the LHC”. In: *Phys. Lett. B* 716 (2012), pp. 1–29. doi: [10.1016/j.physletb.2012.08.020](https://doi.org/10.1016/j.physletb.2012.08.020) (cited on page 1).
- [8] M. Gell-Mann. “A Schematic Model of Baryons and Mesons”. In: *Resonance* 24 (1964), pp. 923–925 (cited on page 1).
- [9] G. Zweig. “An SU(3) model for strong interaction symmetry and its breaking. Version 2”. In: *DEVELOPMENTS IN THE QUARK THEORY OF HADRONS. VOL. 1. 1964 - 1978*. Ed. by D. B. Lichtenberg and S. P. Rosen. Feb. 1964, pp. 22–101 (cited on page 1).
- [10] D. J. Gross and F. Wilczek. “Ultraviolet Behavior of Non-Abelian Gauge Theories”. In: *PRL* 30.26 (June 1973), pp. 1343–1346. doi: [10.1103/PhysRevLett.30.1343](https://doi.org/10.1103/PhysRevLett.30.1343) (cited on page 1).
- [11] C. Giunti and C. W. Kim. *Fundamentals of Neutrino Physics and Astrophysics*. Oxford University Press, Mar. 2007 (cited on page 1).
- [12] M. D. Schwartz. *Quantum Field Theory and the Standard Model*. Cambridge University Press, 2013 (cited on page 1).
- [13] A. Trettin. “Search for eV-scale sterile neutrinos with IceCube DeepCore”. PhD thesis. Berlin, Germany: Humboldt-Universität zu Berlin, Mathematisch-Naturwissenschaftliche Fakultät, 2023. doi: <https://github.com/atrettin/PhD-Thesis> (cited on pages 3, 6).
- [14] N. Deruelle, J.-P. Uzan, and P. de Forcrand-Millard. *Relativity in Modern Physics*. Oxford University Press, Aug. 2018 (cited on page 4).
- [15] R. L. Workman et al. “Review of Particle Physics”. In: *Progress of Theoretical and Experimental Physics* 2022.8 (Aug. 2022), p. 083C01. doi: [10.1093/ptep/ptac097](https://doi.org/10.1093/ptep/ptac097) (cited on pages 4, 23, 24).
- [16] M. Fukugita and T. Yanagida. “Baryogenesis without grand unification”. In: *Physics Letters B* 174.1 (1986), pp. 45–47. doi: [https://doi.org/10.1016/0370-2693\(86\)91126-3](https://doi.org/10.1016/0370-2693(86)91126-3) (cited on page 4).
- [17] R. Davis, D. S. Harmer, and K. C. Hoffman. “Search for Neutrinos from the Sun”. In: *Phys. Rev. Lett.* 20 (21 May 1968), pp. 1205–1209. doi: [10.1103/PhysRevLett.20.1205](https://doi.org/10.1103/PhysRevLett.20.1205) (cited on page 4).

- [18] Y. Fukuda et al. “Evidence for Oscillation of Atmospheric Neutrinos”. In: *Phys. Rev. Lett.* 81 (8 Aug. 1998), pp. 1562–1567. doi: [10.1103/PhysRevLett.81.1562](https://doi.org/10.1103/PhysRevLett.81.1562) (cited on page 4).
- [19] Q. R. Ahmad and other. “Direct Evidence for Neutrino Flavor Transformation from Neutral-Current Interactions in the Sudbury Neutrino Observatory”. In: *Phys. Rev. Lett.* 89 (1 June 2002), p. 011301. doi: [10.1103/PhysRevLett.89.011301](https://doi.org/10.1103/PhysRevLett.89.011301) (cited on page 4).
- [20] S. Alam et al. “Completed SDSS-IV extended Baryon Oscillation Spectroscopic Survey: Cosmological implications from two decades of spectroscopic surveys at the Apache Point Observatory”. In: *Phys. Rev. D* 103 (8 Apr. 2021), p. 083533. doi: [10.1103/PhysRevD.103.083533](https://doi.org/10.1103/PhysRevD.103.083533) (cited on page 4).
- [21] N. Aghanim et al. “Planck2018 results: VI. Cosmological parameters”. In: *Astronomy & Astrophysics* 641 (Sept. 2020), A6. doi: [10.1051/0004-6361/201833910](https://doi.org/10.1051/0004-6361/201833910) (cited on page 4).
- [22] M. Aker et al. “Direct neutrino-mass measurement with sub-electronvolt sensitivity”. In: *Nature Phys.* 18.2 (2022), pp. 160–166. doi: [10.1038/s41567-021-01463-1](https://doi.org/10.1038/s41567-021-01463-1) (cited on page 4).
- [23] T. Asaka, S. Blanchet, and M. Shaposhnikov. “The nuMSM, dark matter and neutrino masses”. In: *Phys. Lett. B* 631 (2005), pp. 151–156. doi: [10.1016/j.physletb.2005.09.070](https://doi.org/10.1016/j.physletb.2005.09.070) (cited on page 6).
- [24] T. Asaka and M. Shaposhnikov. “The  $\nu$ MSM, dark matter and baryon asymmetry of the universe”. In: *Phys. Lett. B* 620 (2005), pp. 17–26. doi: [10.1016/j.physletb.2005.06.020](https://doi.org/10.1016/j.physletb.2005.06.020) (cited on page 6).
- [25] P. Minkowski. “ $\mu \rightarrow e \gamma$  at a rate of one out of  $10^9$  muon decays?” In: *Physics Letters B* 67.4 (Apr. 1977), pp. 421–428. doi: [10.1016/0370-2693\(77\)90435-X](https://doi.org/10.1016/0370-2693(77)90435-X) (cited on page 6).
- [26] T. Yanagida. “Horizontal Symmetry and Masses of Neutrinos”. In: *Progress of Theoretical Physics* 64.3 (Sept. 1980), pp. 1103–1105. doi: [10.1143/PTP.64.1103](https://doi.org/10.1143/PTP.64.1103) (cited on page 6).
- [27] S. L. Glashow. “The Future of Elementary Particle Physics”. In: *NATO Sci. Ser. B* 61 (1980), p. 687. doi: [10.1007/978-1-4684-7197-7\\_15](https://doi.org/10.1007/978-1-4684-7197-7_15) (cited on page 6).
- [28] M. Gell-Mann, P. Ramond, and R. Slansky. “Complex Spinors and Unified Theories”. In: *Conf. Proc. C* 790927 (1979), pp. 315–321 (cited on page 6).
- [29] R. N. Mohapatra and G. Senjanovi ć. “Neutrino Mass and Spontaneous Parity Nonconservation”. In: *Phys. Rev. Lett.* 44 (14 Apr. 1980), pp. 912–915. doi: [10.1103/PhysRevLett.44.912](https://doi.org/10.1103/PhysRevLett.44.912) (cited on page 6).
- [30] M. G. Aartsen et al. “eV-Scale Sterile Neutrino Search Using Eight Years of Atmospheric Muon Neutrino Data from the IceCube Neutrino Observatory”. In: *Phys. Rev. Lett.* 125.14 (2020), p. 141801. doi: [10.1103/PhysRevLett.125.141801](https://doi.org/10.1103/PhysRevLett.125.141801) (cited on page 6).
- [31] J.-L. Tastet, O. Ruchayskiy, and I. Timiryasov. “Reinterpreting the ATLAS bounds on heavy neutral leptons in a realistic neutrino oscillation model”. In: *JHEP* 12 (2021), p. 182. doi: [10.1007/JHEP12\(2021\)182](https://doi.org/10.1007/JHEP12(2021)182) (cited on page 6).
- [32] D. A. Bryman and R. Shrock. “Constraints on Sterile Neutrinos in the MeV to GeV Mass Range”. In: *Phys. Rev. D* 100 (2019), p. 073011. doi: [10.1103/PhysRevD.100.073011](https://doi.org/10.1103/PhysRevD.100.073011) (cited on pages 7, 8).
- [33] A. Aguilar-Arevalo et al. “Improved search for heavy neutrinos in the decay  $\pi \rightarrow e \nu$ ”. In: *Phys. Rev. D* 97.7 (2018), p. 072012. doi: [10.1103/PhysRevD.97.072012](https://doi.org/10.1103/PhysRevD.97.072012) (cited on page 7).
- [34] G. Bellini et al. “New limits on heavy sterile neutrino mixing in B8 decay obtained with the Borexino detector”. In: *Phys. Rev. D* 88.7 (2013), p. 072010. doi: [10.1103/PhysRevD.88.072010](https://doi.org/10.1103/PhysRevD.88.072010) (cited on pages 7, 10).
- [35] D. Britton et al. “Improved search for massive neutrinos in  $\pi^+ \rightarrow e^+ \nu$  decay”. In: *Physical Review D* 46 (1992) (cited on page 7).
- [36] C. J. Parkinson et al. “Search for heavy neutral lepton production at the NA62 experiment”. In: *PoS EPS-HEP2021* (2022), p. 686. doi: [10.22323/1.398.0686](https://doi.org/10.22323/1.398.0686) (cited on pages 7, 8).
- [37] K. Abe et al. “Search for heavy neutrinos with the T2K near detector ND280”. In: *Phys. Rev. D* 100.5 (2019), p. 052006. doi: [10.1103/PhysRevD.100.052006](https://doi.org/10.1103/PhysRevD.100.052006) (cited on pages 7, 8).
- [38] P. Abreu et al. “Search for neutral heavy leptons produced in Z decays”. In: *Z. Phys. C* 74 (1997). [Erratum: *Z. Phys. C* 75, 580 (1997)], pp. 57–71. doi: [10.1007/s002880050370](https://doi.org/10.1007/s002880050370) (cited on pages 7, 9).

- [39] R. Barouki, G. Marocco, and S. Sarkar. “Blast from the past II: Constraints on heavy neutral leptons from the BEBC WA66 beam dump experiment”. In: *SciPost Phys.* 13 (2022), p. 118. doi: [10.21468/SciPostPhys.13.5.118](https://doi.org/10.21468/SciPostPhys.13.5.118) (cited on pages 7–9).
- [40] F. Bergsma et al. “A Search for Decays of Heavy Neutrinos”. In: *Phys. Lett. B* 128 (1983). Ed. by J. Tran Thanh Van, p. 361. doi: [10.1016/0370-2693\(83\)90275-7](https://doi.org/10.1016/0370-2693(83)90275-7) (cited on page 7).
- [41] G. Aad et al. “Search for heavy neutral leptons in decays of  $W$  bosons produced in 13 TeV  $pp$  collisions using prompt and displaced signatures with the ATLAS detector”. In: *JHEP* 10 (2019), p. 265. doi: [10.1007/JHEP10\(2019\)265](https://doi.org/10.1007/JHEP10(2019)265) (cited on pages 7, 8).
- [42] G. Aad et al. “Search for Heavy Neutral Leptons in Decays of  $W$  Bosons Using a Dilepton Displaced Vertex in  $\sqrt{s} = 13\text{TeV}$   $pp$  Collisions with the ATLAS Detector”. In: *Phys. Rev. Lett.* 131 (6 Aug. 2023), p. 061803. doi: [10.1103/PhysRevLett.131.061803](https://doi.org/10.1103/PhysRevLett.131.061803) (cited on pages 7, 8).
- [43] A. M. Sirunyan et al. “Search for heavy neutral leptons in events with three charged leptons in proton-proton collisions at  $\sqrt{s} = 13\text{ TeV}$ ”. In: *Phys. Rev. Lett.* 120.22 (2018), p. 221801. doi: [10.1103/PhysRevLett.120.221801](https://doi.org/10.1103/PhysRevLett.120.221801) (cited on pages 7, 8).
- [44] A. Tumasyan et al. “Search for long-lived heavy neutral leptons with displaced vertices in proton-proton collisions at  $\sqrt{s}=13\text{ TeV}$ ”. In: *JHEP* 07 (2022), p. 081. doi: [10.1007/JHEP07\(2022\)081](https://doi.org/10.1007/JHEP07(2022)081) (cited on pages 7, 8).
- [45] A. Vaitaitis et al. “Search for neutral heavy leptons in a high-energy neutrino beam”. In: *Phys. Rev. Lett.* 83 (1999), pp. 4943–4946. doi: [10.1103/PhysRevLett.83.4943](https://doi.org/10.1103/PhysRevLett.83.4943) (cited on pages 7, 8).
- [46] E. Fernandez-Martinez et al. “Effective portals to heavy neutral leptons”. In: *JHEP* 09 (2023), p. 001. doi: [10.1007/JHEP09\(2023\)001](https://doi.org/10.1007/JHEP09(2023)001) (cited on pages 7–9).
- [47] G. Bernardi et al. “Search for Neutrino Decay”. In: *Phys. Lett. B* 166 (1986), pp. 479–483. doi: [10.1016/0370-2693\(86\)91602-3](https://doi.org/10.1016/0370-2693(86)91602-3) (cited on page 7).
- [48] S. Ito et al. “Search for heavy neutrinos in  $\pi^+ \rightarrow \mu^+ \nu$  decay and status of lepton universality test in the PIENU experiment”. In: *JPS Conf. Proc.* 33 (2021). Ed. by N. Saito, pp. 011131-1–011131-6. doi: [10.7566/JPSCP.33.011131](https://doi.org/10.7566/JPSCP.33.011131) (cited on page 7).
- [49] A. V. Artamonov et al. “Search for heavy neutrinos in  $K^+ \rightarrow \mu^+ \nu_H$  decays”. In: *Phys. Rev. D* 91.5 (2015). [Erratum: *Phys.Rev.D* 91, 059903 (2015)], p. 052001. doi: [10.1103/PhysRevD.91.052001](https://doi.org/10.1103/PhysRevD.91.052001) (cited on pages 7, 8).
- [50] P. Abratenko et al. “Search for Heavy Neutral Leptons in Electron-Positron and Neutral-Pion Final States with the MicroBooNE Detector”. In: *Phys. Rev. Lett.* 132.4 (2024), p. 041801. doi: [10.1103/PhysRevLett.132.041801](https://doi.org/10.1103/PhysRevLett.132.041801) (cited on pages 7, 8).
- [51] P. Astier et al. “Search for heavy neutrinos mixing with tau neutrinos”. In: *Phys. Lett. B* 506 (2001), pp. 27–38. doi: [10.1016/S0370-2693\(01\)00362-8](https://doi.org/10.1016/S0370-2693(01)00362-8) (cited on page 7).
- [52] J. Orloff, A. N. Rozanov, and C. Santoni. “Limits on the mixing of tau neutrino to heavy neutrinos”. In: *Phys. Lett. B* 550 (2002), pp. 8–15. doi: [10.1016/S0370-2693\(02\)02769-7](https://doi.org/10.1016/S0370-2693(02)02769-7) (cited on pages 8, 9).
- [53] I. Boiarska et al. “Constraints from the CHARM experiment on heavy neutral leptons with tau mixing”. In: *Phys. Rev. D* 104.9 (2021), p. 095019. doi: [10.1103/PhysRevD.104.095019](https://doi.org/10.1103/PhysRevD.104.095019) (cited on pages 8, 9).
- [54] A. Cooper-Sarkar et al. “Search for heavy neutrino decays in the BEBC beam dump experiment”. In: *Physics Letters B* 160.1 (1985), pp. 207–211. doi: [https://doi.org/10.1016/0370-2693\(85\)91493-5](https://doi.org/10.1016/0370-2693(85)91493-5) (cited on page 8).
- [55] B. Shuve and M. E. Peskin. “Revision of the LHCb Limit on Majorana Neutrinos”. In: *Phys. Rev. D* 94.11 (2016), p. 113007. doi: [10.1103/PhysRevD.94.113007](https://doi.org/10.1103/PhysRevD.94.113007) (cited on page 8).
- [56] R. Aaij et al. “Search for heavy neutral leptons in  $W^+ \rightarrow \mu^+ \mu^\pm \text{jet}$  decays”. In: *Eur. Phys. J. C* 81.3 (2021), p. 248. doi: [10.1140/epjc/s10052-021-08973-5](https://doi.org/10.1140/epjc/s10052-021-08973-5) (cited on page 8).
- [57] R. Plestid. “Luminous solar neutrinos I: Dipole portals”. In: *Phys. Rev. D* 104 (2021), p. 075027. doi: [10.1103/PhysRevD.104.075027](https://doi.org/10.1103/PhysRevD.104.075027) (cited on pages 9, 10).

- [58] A. Osipowicz et al. “KATRIN: A Next generation tritium beta decay experiment with sub-eV sensitivity for the electron neutrino mass. Letter of intent”. In: (Sept. 2001) (cited on page 9).
- [59] S. Mertens et al. “A novel detector system for KATRIN to search for keV-scale sterile neutrinos”. In: *Journal of Physics G: Nuclear and Particle Physics* 46.6 (2019), p. 065203. doi: [10.1088/1361-6471/ab12fe](https://doi.org/10.1088/1361-6471/ab12fe) (cited on page 9).
- [60] M. Aker et al. “Search for keV-scale sterile neutrinos with the first KATRIN data”. In: *Eur. Phys. J. C* 83.8 (2023), p. 763. doi: [10.1140/epjc/s10052-023-11818-y](https://doi.org/10.1140/epjc/s10052-023-11818-y) (cited on page 9).
- [61] B. Abi et al. “Deep Underground Neutrino Experiment (DUNE), Far Detector Technical Design Report, Volume II: DUNE Physics”. In: (Feb. 2020) (cited on page 9).
- [62] S. Friedrich et al. “Limits on the Existence of sub-MeV Sterile Neutrinos from the Decay of  $^7\text{Be}$  in Superconducting Quantum Sensors”. In: *Phys. Rev. Lett.* 126.2 (2021), p. 021803. doi: [10.1103/PhysRevLett.126.021803](https://doi.org/10.1103/PhysRevLett.126.021803) (cited on page 9).
- [63] C. Hagner et al. “Experimental search for the neutrino decay  $\nu_3 + \nu_j + e^+ + e^-$  and limits on neutrino mixing”. English. In: 52.3 (1995), pp. 1343–1352. doi: [10.1103/PhysRevD.52.1343](https://doi.org/10.1103/PhysRevD.52.1343) (cited on page 9).
- [64] R. Plestid. “Luminous solar neutrinos II: Mass-mixing portals”. In: *Phys. Rev. D* 104 (2021). [Erratum: *Phys. Rev. D* 105, 099901 (2022)], p. 075028. doi: [10.1103/PhysRevD.104.075028](https://doi.org/10.1103/PhysRevD.104.075028) (cited on page 10).
- [65] P. Coloma et al. “Double-Cascade Events from New Physics in Icecube”. In: *Phys. Rev. Lett.* 119.20 (2017), p. 201804. doi: [10.1103/PhysRevLett.119.201804](https://doi.org/10.1103/PhysRevLett.119.201804) (cited on page 10).
- [66] P. Coloma. “Icecube/DeepCore tests for novel explanations of the MiniBooNE anomaly”. In: *Eur. Phys. J. C* 79.9 (2019), p. 748. doi: [10.1140/epjc/s10052-019-7256-8](https://doi.org/10.1140/epjc/s10052-019-7256-8) (cited on page 10).
- [67] M. Atkinson et al. “Heavy Neutrino Searches through Double-Bang Events at Super-Kamiokande, DUNE, and Hyper-Kamiokande”. In: *JHEP* 04 (2022), p. 174. doi: [10.1007/JHEP04\(2022\)174](https://doi.org/10.1007/JHEP04(2022)174) (cited on page 10).
- [68] P. Coloma et al. “GeV-scale neutrinos: interactions with mesons and DUNE sensitivity”. In: *Eur. Phys. J. C* 81.1 (2021), p. 78. doi: [10.1140/epjc/s10052-021-08861-y](https://doi.org/10.1140/epjc/s10052-021-08861-y) (cited on pages 10, 16).
- [69] M. Tanabashi et al. “Review of Particle Physics”. In: *Phys. Rev. D* 98 (3 Aug. 2018), p. 030001. doi: [10.1103/PhysRevD.98.030001](https://doi.org/10.1103/PhysRevD.98.030001) (cited on pages 11, 13, 24).
- [70] M. Honda et al. “Atmospheric neutrino flux calculation using the NRLMSISE-00 atmospheric model”. In: *Phys. Rev. D* 92 (2 July 2015), p. 023004. doi: [10.1103/PhysRevD.92.023004](https://doi.org/10.1103/PhysRevD.92.023004) (cited on page 11).
- [71] A. Fedynitch et al. “Calculation of conventional and prompt lepton fluxes at very high energy”. In: *European Physical Journal Web of Conferences*. Vol. 99. European Physical Journal Web of Conferences. Aug. 2015, p. 08001. doi: [10.1051/epjconf/20159908001](https://doi.org/10.1051/epjconf/20159908001) (cited on page 12).
- [72] P. A. M. Dirac. “The Quantum Theory of the Emission and Absorption of Radiation”. In: *Proceedings of the Royal Society of London Series A* 114.767 (Mar. 1927), pp. 243–265. doi: [10.1098/rspa.1927.0039](https://doi.org/10.1098/rspa.1927.0039) (cited on page 12).
- [73] I. Esteban et al. “The fate of hints: updated global analysis of three-flavor neutrino oscillations”. In: *JHEP* 09 (2020), p. 178. doi: [10.1007/JHEP09\(2020\)178](https://doi.org/10.1007/JHEP09(2020)178) (cited on page 13).
- [74] A. Terliuk. “Measurement of atmospheric neutrino oscillations and search for sterile neutrino mixing with IceCube DeepCore”. PhD thesis. Berlin, Germany: Humboldt-Universität zu Berlin, Mathematisch-Naturwissenschaftliche Fakultät, 2018. doi: [10.18452/19304](https://doi.org/10.18452/19304) (cited on pages 14, 26).
- [75] J. A. Formaggio and G. P. Zeller. “From eV to EeV: Neutrino cross sections across energy scales”. In: *Rev. Mod. Phys.* 84 (3 Sept. 2012), pp. 1307–1341. doi: [10.1103/RevModPhys.84.1307](https://doi.org/10.1103/RevModPhys.84.1307) (cited on page 15).
- [76] M. G. Aartsen et al. “The IceCube Neutrino Observatory: instrumentation and online systems”. In: *Journal of Instrumentation* 12.3 (Mar. 2017), P03012. doi: [10.1088/1748-0221/12/03/P03012](https://doi.org/10.1088/1748-0221/12/03/P03012) (cited on pages 19, 21).
- [77] P. B. Price, K. Woschnagg, and D. Chirkin. “Age vs depth of glacial ice at South Pole”. In: *Geophysical Research Letters* 27.14 (2000), pp. 2129–2132. doi: <https://doi.org/10.1029/2000GL011351> (cited on page 20).



- [78] R. Abbasi et al. "In-situ estimation of ice crystal properties at the South Pole using LED calibration data from the IceCube Neutrino Observatory". In: *The Cryosphere Discussions* 2022 (2022), pp. 1–48. doi: [10.5194/tc-2022-174](https://doi.org/10.5194/tc-2022-174) (cited on page 20).
- [79] R. Abbasi et al. "The IceCube data acquisition system: Signal capture, digitization, and timestamping". In: *Nuclear Instruments and Methods in Physics Research Section A: Accelerators, Spectrometers, Detectors and Associated Equipment* 601.3 (2009), pp. 294–316. doi: <https://doi.org/10.1016/j.nima.2009.01.001> (cited on pages 20, 21).
- [80] M. G. Aartsen et al. "Energy Reconstruction Methods in the IceCube Neutrino Telescope". In: *JINST* 9 (2014), P03009. doi: [10.1088/1748-0221/9/03/P03009](https://doi.org/10.1088/1748-0221/9/03/P03009) (cited on page 21).
- [81] J. Feintzeig. "Searches for Point-like Sources of Astrophysical Neutrinos with the IceCube Neutrino Observatory". PhD thesis. University of Wisconsin, Madison, Jan. 2014 (cited on page 21).
- [82] N. Kulacz. "In Situ Measurement of the IceCube DOM Efficiency Factor Using Atmospheric Minimum Ionizing Muons". MA thesis. University of Alberta, 2019 (cited on page 21).
- [83] R. Abbasi et al. "The design and performance of IceCube DeepCore". In: *Astropart. Phys.* 35.10 (2012), pp. 615–624. doi: [10.1016/j.astropartphys.2012.01.004](https://doi.org/10.1016/j.astropartphys.2012.01.004) (cited on page 22).
- [84] P. A. Cherenkov. "Visible Radiation Produced by Electrons Moving in a Medium with Velocities Exceeding that of Light". In: *Phys. Rev.* 52 (4 Aug. 1937), pp. 378–379. doi: [10.1103/PhysRev.52.378](https://doi.org/10.1103/PhysRev.52.378) (cited on page 23).
- [85] V. F. Petrenko and R. W. Whitworth. "214Optical and electronic properties". In: *Physics of Ice*. Oxford University Press, Jan. 2002. doi: [10.1093/acprof:oso/9780198518945.003.0009](https://doi.org/10.1093/acprof:oso/9780198518945.003.0009) (cited on page 23).
- [86] I. Frank and I. Tamm. "Coherent visible radiation from fast electrons passing through matter". In: *C. R. Acad. Sci. USSR* 14 (1937), pp. 109–114 (cited on page 23).
- [87] I. Tamm. "Radiation Emitted by Uniformly Moving Electrons". In: *Selected Papers*. Ed. by B. M. Bolotovskii, V. Y. Frenkel, and R. Peierls. Berlin, Heidelberg: Springer Berlin Heidelberg, 1991, pp. 37–53. doi: [10.1007/978-3-642-74626-0\\_3](https://doi.org/10.1007/978-3-642-74626-0_3) (cited on page 23).
- [88] L. Rädcl and C. Wiebusch. "Calculation of the Cherenkov light yield from low energetic secondary particles accompanying high-energy muons in ice and water with Geant4 simulations". In: *Astroparticle Physics* 38 (Oct. 2012), pp. 53–67. doi: [10.1016/j.astropartphys.2012.09.008](https://doi.org/10.1016/j.astropartphys.2012.09.008) (cited on page 23).
- [89] D. Chirkin and W. Rhode. "Propagating leptons through matter with Muon Monte Carlo (MMC)". In: (July 2004) (cited on page 24).
- [90] L. Raedel. "Simulation Studies of the Cherenkov Light Yield from Relativistic Particles in High-Energy Neutrino Telescopes with Geant4". MA thesis. Aachen, Germany: Rheinisch-Westfälischen Technischen Hochschule, 2012 (cited on pages 24, 25).
- [91] E. Longo and I. Sestili. "Monte Carlo Calculation of Photon Initiated Electromagnetic Showers in Lead Glass". In: *Nucl. Instrum. Meth.* 128 (1975). [Erratum: *Nucl.Instrum.Meth.* 135, 587 (1976)], p. 283. doi: [10.1016/0029-554X\(75\)90679-5](https://doi.org/10.1016/0029-554X(75)90679-5) (cited on page 24).
- [92] S. Agostinelli et al. "Geant4—a simulation toolkit". In: *Nucl. Instr. Meth. Phys. Res.* 506.3 (July 2003), pp. 250–303. doi: [10.1016/S0168-9002\(03\)01368-8](https://doi.org/10.1016/S0168-9002(03)01368-8) (cited on page 24).
- [93] T. Gabriel et al. "Energy dependence of hadronic activity". In: *Nuclear Instruments and Methods in Physics Research Section A: Accelerators, Spectrometers, Detectors and Associated Equipment* 338.2 (1994), pp. 336–347. doi: [https://doi.org/10.1016/0168-9002\(94\)91317-X](https://doi.org/10.1016/0168-9002(94)91317-X) (cited on page 25).